From the Plant Layouts to Optimized LP and 3D PWR-KWU Containment Models for Combustion Risk Assessment with GOTHIC8.3 (QA)

L. Serra ^{1*}, A. Domínguez-Bugarín¹, G. Jiménez¹, C. Vázquez-Rodríguez², M. Braun³, S. Kelm², L.E. Herranz⁴

1 Universidad Politécnica de Madrid 28040 Madrid, Spain; 2 Forschungszentrum Juelich, 42425 Juelich, Germany; 3 Framatome GmbH, Paul-Gossen-Strasse 100, D-91052 Erlangen, Germany 4 CIEMAT, 28040 Madrid, Spain

*Corresponding author: luis.slopez@upm.es

ABSTRACT

One of the key objectives of the severe accident management strategies is to preserve containment integrity and to prevent a large release of radioactive products into the environment. To evaluate containment response during a severe accident, two GOTHIC 8.3(QA) models (LP and 3D) of a PWR-KWU containment have been developed in the framework of AMHYCO (EU-funded Horizon 2020 project). The LP and 3D models were compared for the in-vessel phase of a total loss of AC power scenario (SBO), with and without considering Passive Autocatalytic Recombiners (PARs). The two models showed consistent global trends, but the 3D model revealed local variations in hydrogen stratification, condensation, and temperature gradients that were not captured by the LP model. 3D results also highlighted the influence of 3D mesh resolution on stratification and flammability conditions, with finer meshes predicting different hydrogen accumulation flow patterns. As expected, PARs effectively reduced flammable volumes in both models, although 3D models yielded lower recombination rates due to local heterogeneities. Last, this study emphasizes the importance of the post-processing choices made by the user to identify safety relevant conditions with the potential to enhance accident management measures and the positioning of safety systems.

Keywords: KWU, Severe Accident, GOTHIC, Containment, Thermal-hydraulics, PARs

1. INTRODUCTION

Nuclear power plant (NPP) containments are buildings with complex geometries and large internal volumes, which act as the last physical airtight barrier to prevent the release of radioactive fission products to the environment in case of a postulated accident (OECD, 2014). These structures are designed to withstand high pressure and temperature peaks that can be developed in case of a design-basis accident (DBA) or a severe accident (SA). There, complex flow and transport processes are expected to take place within the numerous compartments of the containment. These flows are particularly relevant when hydrogen (H₂) is released from the reactor coolant system (in-vessel phase), or the reactor cavity (ex-vessel phase) and can accumulate or stratify at different locations and elevations within the containment free volume. If the composition of the hydrogen—steam—air mixture lies within certain limits, a combustion event may occur (Sehgal, 2012). In this case, the pressure spike could threaten the containment integrity, depending on the amount of H₂ burned and

the combustion regime. This regime is influenced by factors such as flammable cloud gas concentrations, total volume of combustible gases, and turbulence effects (OECD/NEA, 2000). To mitigate the risk of H₂ combustion, NPPs in several countries have introduced passive autocatalytic recombiners (PARs). These devices slowly but continuously consume H₂ and CO, as long as oxygen is present in the atmosphere, releasing steam, CO₂, and heat (Malakhov et al., 2024).

To evaluate hazardous conditions within the containment compartments, detailed analyses are made in the frame of the Final Safety Analysis Report and the Probabilistic Safety Analysis Level 2. Traditionally, these studies have been performed using computational tools based on the Lumped Parameter (LP) approach. For an LP code, the containment is represented as a network of interconnected control volumes (CVs) with presumably homogeneous thermodynamic conditions, requiring low computational cost (OECD/NEA, 2014a). However, LP codes need to apply several assumptions (e.g., empirical correlations) to simulate large Mass and Energy (M&E) releases and fluid-to-structure interactions with different characteristic lengths (such as convection, condensation or wall friction) in order to deliver an acceptable bounding result (Ofstun and Scobel, 2006; Vazquez-Rodriguez et al., 2019). For instance, LP codes like MELCOR (Humphries et al., 2017) or COCOSYS (Allelein et al., 2008), assume instantaneous mixing within each Control Volume (CV), which neglects three-dimensional effects, reduces spatial resolution, and implies that all the thermal structures within a CV are available to transfer heat at each simulation time step (Ofstun et al., 2013).

The expansion of computational capabilities in the last two decades has boosted the use of codes which are able to solve the conservation equations in three dimensions. These 3D and Computational Fluid Dynamic (CFD) codes allow to capture local effects and flow patterns, as momentum's direction is conserved and turbulence terms are included in the solver (Wolf et al., 1999). Moreover, although the higher thermal-hydraulic resolution implies a higher computational cost, if an adequate mesh is implemented, they could have affordable computational costs. Additionally, 3D codes such as GOTHIC (EPRI, 2018) can support mixed 3D-LP calculations where the modeler can zoom into critical areas where local phenomena like H₂ pockets, stratification, or jet impingement are important (OECD/NEA, 2014b). Especially since the Fukushima Daiichi accident, 3D and CFD models have provided valuable insights into the effectiveness of severe accident management actions and their impact on containment conditions. Nevertheless, simulating a full severe accident sequence from initiating event to the final state is still very challenging both for 3D and CFD codes.

Several studies in public Literature have modeled previously the KraftWerk Union AG Pressurized Water Reactor (PWR-KWU) containment, known for its high compartmentalization and numerous non-orthogonal walls. The earliest examples is the simulation of a full SA with GASFLOW, using a 3D cartesian mesh with 180.000 cells by the Karlsruhe Institute of Technology (Royl et al., 2000). The model was successful in predicting large buoyant and convective jets of steam, stratification of gas clouds, and the role of combustion risk mitigation measures. Also, the model was compared to a parallel LP simulation with 100 nodes, which couldn't predict H2 stratification and local gas temperatures. Other examples are the use of GASFLOW coupled with MELCOR simulating a LOCA scenario in a generic PWR-KWU (Szabó et al., 2014), or the plant-scale 3D simulation of Borssele NPP with ANSYS FLUENT, assessing H₂ risk and mitigation systems during an Intermediate-Break LOCA (Visser et al., 2015). Moreover, in the last decade, GOTHIC has been used to develop 3D evaluation models of PWR-KWU containments. One example is the construction of a hybrid LP-3D model to simulate a fast release of H2-steam mixture during a Station Black Out (SBO) and to study H₂ accumulation to test a PAR layout, with special focus on the preferential H₂ pathways and accumulation zones (Lopez-Alonso et al., 2017; Papini et al., 2019, 2015). Another example is the development of a 3D PWR-KWU 3 loops model of Trillo NPP, where a novel procedure is proposed by adapting a previously detailed Computer-Aided Design (CAD) geometry over an adequate mesh (Fernández-Cosials et al., 2019).

Recently, the combined use of LP, 3D and CFD codes for the simulation of long accident sequences in large-dry containments has been a key goal of the H2020 AMHYCO project (Herranz et al., 2025, 2022; Jimenez et al., 2022). Its main objective was to improve experimental knowledge and simulation capabilities for the H2/CO combustion risk management in a SA. To achieve this goal, detailed CAD models of three PWR containments (Western, KWU, and VVER) were used to create a unique database of containment specifications to assure certain code-to-code comparability and to make optimal use of the connection between the three simulation approaches. That allowed, in a later phase, to identify interesting sequences for 3D codes and specific time windows for CFD simulations, which could unmask possible harsher conditions regarding non-condensable gases (NCGs) accumulation, combustible clouds, or higher temperature pockets that may be hidden by a coarser modelling.

Nonetheless, building 3D models is still a time-consuming task, especially regarding the election of a sufficiently fine discretization of the calculation domain featuring all the complex configurations of the geometry (Yu et al., 2018). Normally, the mesh generation and the successful fitting of the geometry requires more than 40% of a 3D containment analysis campaign (Fernández-Cosials et al., 2019). This issue has influenced some research groups to develop methodologies towards the enhancement of the model's computational robustness, balancing the representation of relevant geometric aspects and the computational cost (Bocanegra et al., 2016; Vázquez-Rodríguez et al., 2025; Xiao et al., 2016). Optimizing the construction of detailed yet efficient 3D models is crucial for improving accident thermal-hydraulic studies and developing effective safety measures (EPRI, 2015).

Moreover, key differences between LP and 3D models—arising from their underlying assumptions and approximations—remain insufficiently quantified, particularly in the treatment of critical containment phenomena such as H₂ stratification, mixing, and combustion. This paper aims to readdress this gap by performing a detailed comparison study between an LP and an equivalent 3D model of a PWR-KWU containment with the GOTHIC code. An examination of how the choice of modeling approach (LP vs. 3D) affects the representation of H₂ risk and thermal hydraulics is performed, identifying differences that stem from modelling approaches rather than intrinsic code or geometric dissimilarities. This will be done by studying how different resolution in the 3D models, and on the post-processing of the results, can impact the characterization of a simulation. In detail, the LP CVs are compared with their equivalent 3D cell regions, followed by a comparison of 3D regions with smaller compartments and selected individual cell data. The goal is to improve containment modeling strategies and enhance accident management measures.

In Section 2 of this paper, the construction of the detailed CAD PWR-KWU from available layouts is shown, together with the methodologies followed to extract all parameters needed for simulation and the different volume nodalization approaches. Section 3 describes the transference of the containment geometry into the GOTHIC LP and 3D models. Section 4 presents the simulation results of the containment response to the in-vessel phase of a SBO sequence, as studied during the AMHYCO project. Two variants of the accident sequence were simulated, an unmitigated case, and one mitigated case where PARs are installed in the containment.

2. PWR-KWU 3D CAD CONTAINMENT MODEL

2.1 Detailed containment geometry and extraction of specifications per region and room

The modelled PWR-KWU containment corresponds to a 1300 MWe KONVOI-type reactor from the cancelled Stendal NPP site (SIEMENS, 1990). The building consists of a spherical steel containment (UJA) and a surrounding reinforced-concrete airplane crash shell (UJB). The UJA containment is divided into the accessible rooms (during power operation) and the equipment rooms housing the

reactor coolant system (in green and red, respectively, in Fig. 1-left). These equipment rooms are surrounded by a concrete shrapnel cylinder that encloses the sump, reactor pressure vessel (RPV), and several measurement and small-equipment rooms. One noticeable aspect is the high compartmentalization and the existence of numerous relatively thin concrete walls. This complex geometry considers radioactive protection, as well as equipment transport paths and personnel escape routes. The bottom-to-top CAD construction was undertaken by extruding walls and floors over the available 2D layouts and identifying all the connections between compartments. Fig. 1-right depicts the complete UJA model (excluding the spherical steel shell), where the large in-containment steel structures can be seen (e.g., the polar crane). The modelling of the metallic components relied mostly upon detailed plans, although approximate shapes were used while maintaining the actual disposition and dimensions of the supports and platforms.

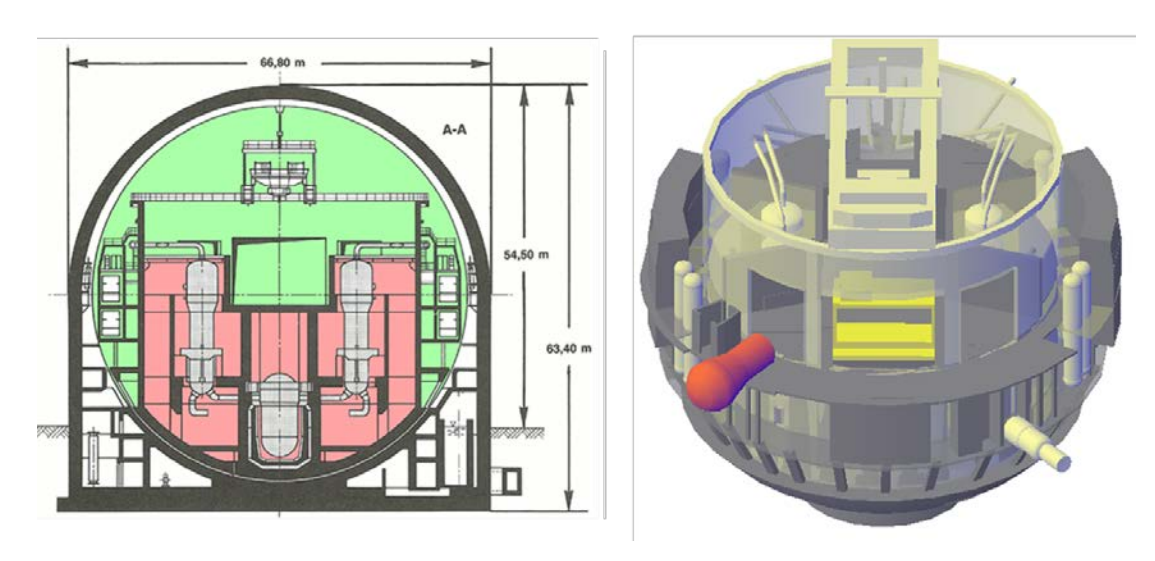


Fig. 1. PWR-KWU containment accessible (green) and equipment rooms (red) layout (left), and full UJA containment model (right).

The detailed geometry was then dissected into a 'Generic Containment' database (Serra et al., 2023), envisaged during AMHYCO Work Package (WP) 2 to maximize the code-to-code comparability between different approaches. First, the zones of the containment which likely behave in a similar way under accident conditions, are grouped together in so-called *regions*. For an LP code, these regions correspond to the CVs. Also, a region for the UJB containment building was included, as this volume would account for the main heat loss of the containment in the case of a SA. Table 1 gathers free volume and heat structure (HS) surfaces (concrete and steel of non-insulated equipment) per region. For each group of HSs, the total volume and surface area is determined by lumping adjacent structures from the CAD. Thicknesses are then deduced by dividing the HS volume by its surface area (Dominion, 2006).

The 10 UJA regions were further divided into 38 smaller spaces, from now on called *rooms*, identified in the available layouts. This classification represents the actual physical separation of the different compartments, such as the instrumentation chambers or the pressurizer tower, and will be used at the post-processing stages. For that, the relative coordinates of the rooms, within their mother regions, need to be defined. Also, the approximate location of 13 sensors (temperature measurements and the in-situ containment atmosphere H₂ monitoring system) was identified (FRAMATOME, 2024a; SIEMENS, 1990). Fig. 2. depicts cuts through the containment, representing the regions by color, the rooms by white boxes with numbers, and the locations of the measurement

points by yellow rhombi. For example, one monitor is installed close to each reactor coolant system (RCS) loop to detect H_2 near the potential leakage locations, while a pair of monitors are installed around the pressurizer, to register a H_2 release via a primary depressurization. The knowledge of the position of these sensors allows for a comparison of the simulated atmosphere in the entire containment, and what limited information the main control room would have access to.

Table 1. PWR	-K\\\\\ C	nntainment	enecifications	ner region
Table I. F WIN	11 0 0 0 00	JIIIAIIIIIIGIII	Specifications	per region

Region	Nomenclature	Free Volume (m³)	Concrete floor surface (m²)	Concrete wall surface (m²)	Steel wall surface (m²)
1	Cavity (CAV)	205	68	833	0
2	Sump (SUMP)	5132	1871	2914	5396
3	Pipeline Duct (DUCT)	2668	1024	1417	968
4	Steam Generators – North (SG-N)	4551	550	2466	6129
5	Steam Generators – South (SG-S)	4489	531	2387	6169
6	Annular compartments- East (ANN-E)	6091	2403	3798	2098
7	Annular compartments- West (ANN-W)	5783	2170	3787	2154
8	Spent Fuel Pool (SFP)	1327	97	477	0
9	Reactor Room (RROOM)	1044	310	588	0
10	Dome (DOME)	42654	1870	6743	9193
11	UJB building	49255	9781	20487	7923
Total		123199	20675	45897	40030

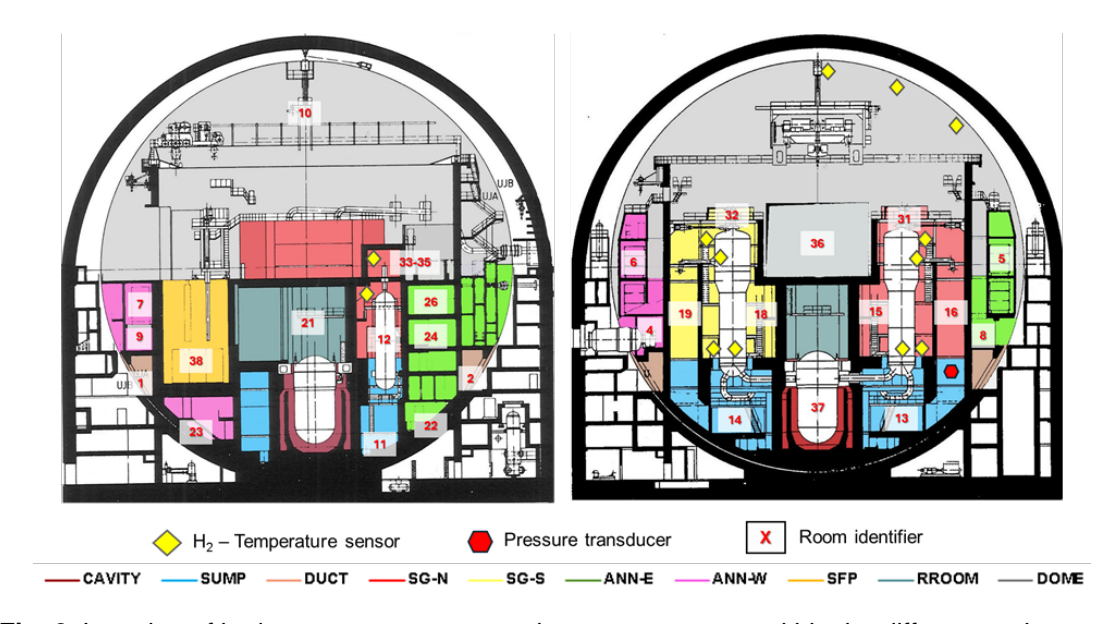


Fig. 2. Location of hydrogen, temperature and pressure sensors within the different regions and rooms of the containment.

Finally, a non-plant-specific 40-PAR layout is proposed, based on 20 Framatome FR-1500 and 20 FR-960 (FRAMATOME, 2024b). This recombination capacity is comparable to the values in other references for the same containment design (Kelm, 2019; Royl et al., 2000). Also, PAR positioning was undertaken on the basis of IAEA's recommendations (IAEA, 2011). For instance, spaces close to H₂ releases, and where combustible gases ascend, are equipped with a higher number of PARs. Fig. 3 depicts the location of 19 PARs at different regions at the +12-meter elevation, and another set

of 9 PARs at the elevation of the operational floor. The layout is completed with 4 PARs both at the sump and duct regions at +6-meter elevation, and 4 more units located at the polar crane in the upper dome.

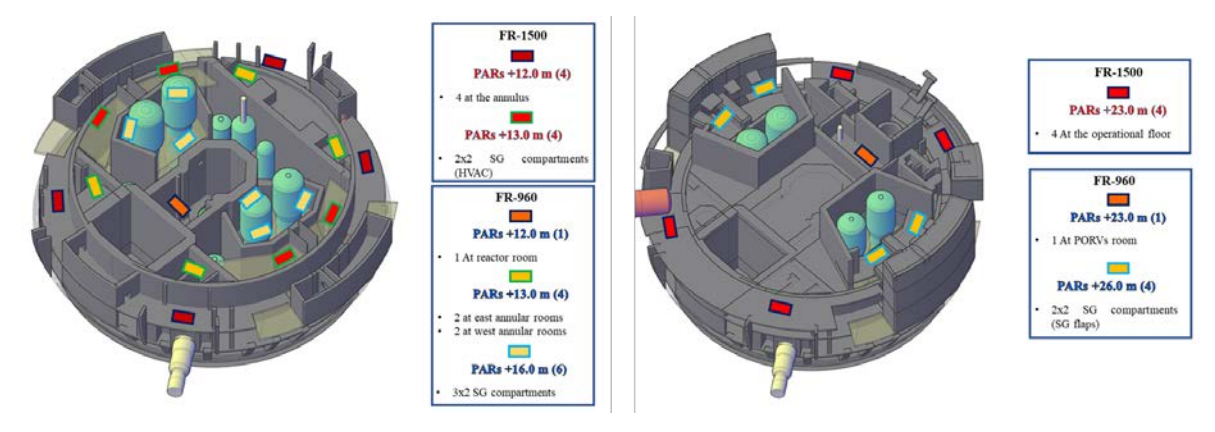


Fig. 3. PAR layout (not complete) at +12 m elevation (left), and above the operational floor (right).

3. PWR-KWU CONTAINMENT MODELING WITH THE GOTHIC CODE

3.1 The GOTHIC 8.3(QA) code

GOTHIC is an integrated, general-purpose multi-physics software package that solves mass, momentum and energy conservation equations for multi-component and multi-phase flow (EPRI, 2018). The code can be used to model both LP and 3D volumes, as well as a combination in a hybrid domain-decomposition approach. This provides modelling flexibility, balancing between computational cost and accuracy for regions with higher or lower impact in terms of system response and feedback effects (Harvill et al., 2021). Unlike CFD codes which implement body-fitting meshes on the geometry, GOTHIC uses a porous-media approach to represent the geometry within a userdefined Cartesian mesh and by using specific types of geometric blockages and openings. A volumetric porosity factor is assigned to each cell in the mesh to define whether the cell is partially open or closed, while a surface porosity factor is applied at each cell face, which determines the hydraulic separation between adjacent cells. Regarding the representation of HSs, nodalized Thermal Conductors (TCs) are used to model heat transfer between solid and fluid through the different walls and floors. The heat diffusion on the solid side is calculated based on a finite-difference 1D model, while the heat transfer coefficient options are applied at the surfaces by user-specified values and built-in engineering correlations. For condensation in the presence of NCGs, the proprietary diffusion layer model (DLM), formulated based on a heat/mass transfer analogy, is selected.

3.2 LP model based on a Generic Containment approach

The LP GOTHIC model was directly built based on the developed database. The free volume of the 11 regions and the 24 flow paths connecting them were transferred as inputs in corresponding CVs. This lumped nodalization corresponds to the regions shown on Fig. 2. Moreover, for each pressure-dependent junction, a valve component was defined with opening trips. The 71 HSs of the database were transformed into TCs, conserving realistic surface-to-volume ratios and the mass of material internally calculated by the code when multiplying the given thickness and surface area. Regarding the implementation of the PAR layout, 40 flow paths are defined in the corresponding CVs. These represent the open space inside the PAR box, whereas a built-in PAR component is placed on them to model the recombination process and estimate the buoyant plume. The PAR component definition

also requires input such as the startup and shutdown H_2 fractions for PAR operation, a heat loss factor from the PAR, and the recombination efficiency. The latter is provided by control variables coupled with an external Dynamically Linked Library (DLL), which updates the value based on the local conditions (e.g., gas density, volumetric fractions and temperature, flow velocity) at the entrance of the PAR at each time step. The DLL contains several correlations depending on the PAR type, and its coefficients have been adjusted in the framework of the AMHYCO project (Braun and Reinecke, Preprint Available at SSRN: https://ssrn.com/abstract=5199266).

3.3 3D model based on the "Preventive Methodology"

The adaptation of the CAD to a 3D GOTHIC model was undertaken in several steps. Firstly, the detailed geometry was simplified, maintaining as far as possible the thicknesses, areas and volumes. This was performed under the 'Preventive Methodology', which consist of adapting the geometry to previously chosen meshes so that the blocks imported as input (mainly prisms and wedges) do not generate problematic cells in GOTHIC (Vázquez-Rodríguez et al., 2025). With this method, models with several compatible homogeneous meshes can be implemented, proving to be sufficiently efficient to run longer transients than with previous approaches. In this case, homogeneous meshes with a resolution of 8 m³, 1 m³ and 0.125 m³ per cell were used. Moreover, the simplified and mesh-adapted walls need to guarantee the hydraulic independence between rooms, i.e., that no flow could be able to penetrate the modelled walls through any undesired spot. To achieve that, leaning walls were rectangularized, and cell faces had to be completely blocked wherever the structure fully separated fluid regions. While the Preventive Methodology is better depicted in (Vázquez-Rodríguez et al., 2025), Fig. 4 depicts the simplified UJA containment and exemplifies the simplification of the geometry over the mesh. The methodology has proved to decrease the computational cost of the GOTHIC models by a factor of 40.

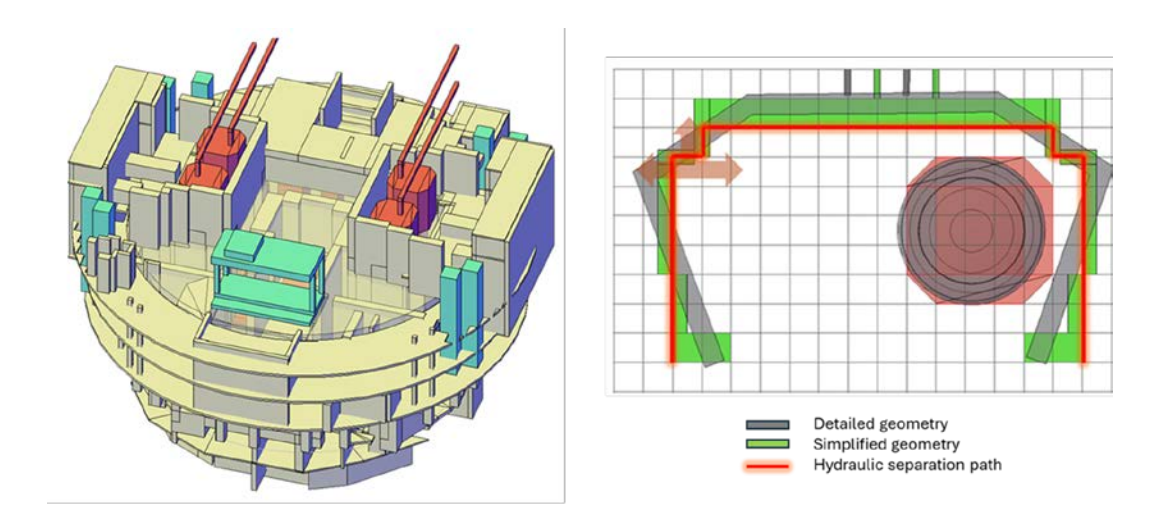


Fig. 4. Simplified UJA containment model (left), reconstruction of the detailed geometry over a homogeneous mesh respecting the hydraulic independence (right).

To represent the geometry in GOTHIC, a hybrid approach was conceived. Firstly, although all blocks could be allocated in one subdivided volume, they were split into three CVs, which separate the UJA accessible and equipment rooms inside/outside the cylinder. Within these subdivided CVs, 8 of the 11 LP regions are represented. The other 3, namely SFP, CAV and UJB volumes, were defined as

LP CVs. This was done to facilitate the modelling of the M&E sources in the cavity, the pool heat sink (as to include the possible long-term boiling in the late phase of accidents), and the major heat loss of the containment in case of a SA via the outer containment shell. Then, in a first meshing approach, the volume for the equipment rooms was outfitted with a 1 m³ per cell mesh to better capture the conditions near the break locations at the RCS or the cavity. An exception was made in the first levels of the containment sump, where a 4-meter-high first row of cells was imposed to ensure the liquid level remained within it throughout the transient, thereby avoiding numerical instabilities in GOTHIC 8.3(QA) and earlier versions when the water level crosses a z-grid line—an issue resolved in more recent versions. Then, the two subdivided volumes for the accessible rooms used a coarser mesh (8 m³ per cell) to reduce the computational effort in long simulation runs. This model is later referred to as "3D-60k". Beside this "baseline" model, two additional models were created by re-meshing (Table 2). The "3D-30k" model used a coarser mesh in the equipment rooms (8 m³ per cell). The "3D-80K" model used a finer mesh (1 m³ per cell) in the accessible rooms which lay inside the shrapnel cylinder above the operational floor. These 3D models would then be subjected to a comparison of their computational robustness, and the gain/loss of details achieved with finer or coarser meshes. The mesh resolution and the total number of active cells of the 3D models is gathered in Table 2, while Fig. 5 shows the arrangement of CVs in both GOTHIC LP and 3D models at the graphic user interface.

Table 2. Resolution and number of cells of the 3D models.

3D model	'3D-30k'	'3D-60k'	'3D-80k'
Mesh resolution accessible rooms (on the operational floor)	8 m ³	8 m ³	1 m ³
Mesh resolution accessible rooms (outside cylinder)	8 m ³	8 m ³	8 m ³
Mesh resolution equipment rooms	8 m ³	1 m ³	1 m ³
Total number of cells	31250	60320	82450
Active cells	11391	25225	41134

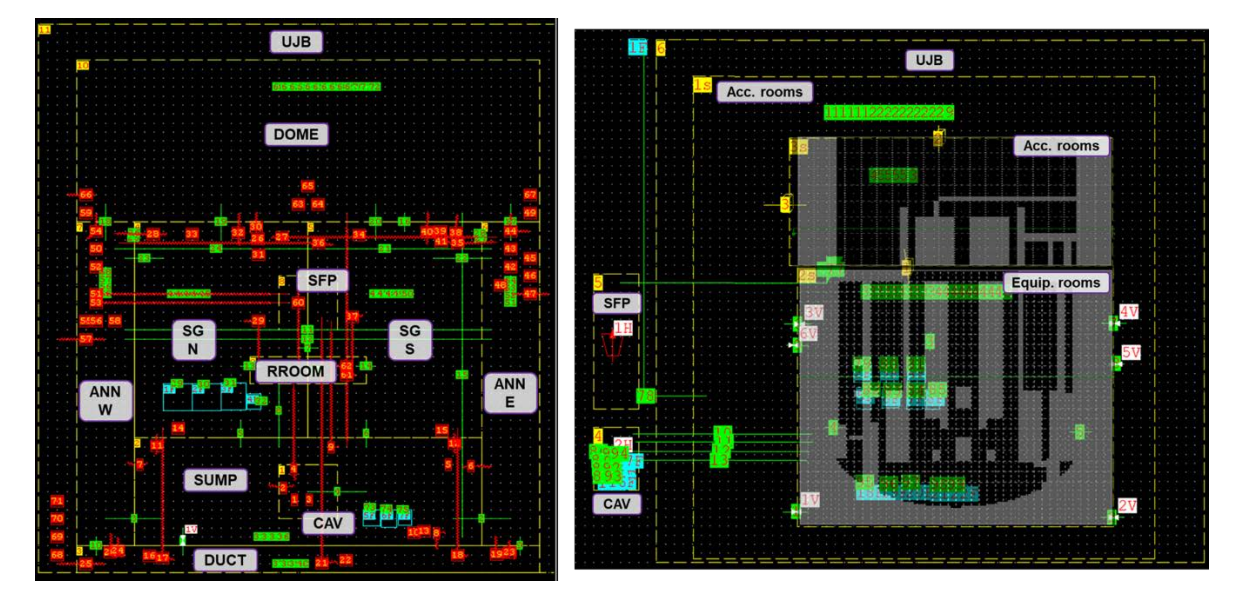


Fig. 5. Arrangement of control volumes and built-in modelling tools at GOTHIC LP model (left) and 3D model (right).

Regarding the implementation of the 71 HSs of the database, the 3D models gather a total of 529 TCs, the majority being located over the cells directly adjacent to each wall and floor exposed to the fluid. Table 3 shows the agreement between the database specifications, the LP model and the GOTHIC 3D implementation in terms of containment free volume, integrated structure mass, volume and area, together with the material properties of the concrete and steel defined as material layers at the TCs (Serra et al., 2023). The aforementioned comparison is needed to demonstrate that the geometry adaptation would not compromise the evaluation of the containment characteristics between different approaches. Finally, regarding the implementation of the PAR layout, and differently from the LP implementation, forty 1 m³ blocks are implemented in the geometry, approximately considering the space occupied by the PAR metallic housings. Then, 40 flow paths are defined as traversing those blocks, with their lower and upper elevations matching the cells where the PAR inlets and outlets are located.

Table 3. Integrated heat structure mass, volume and area at UJA containment: Database vs. GOTHIC LP vs GOTHIC 3D. Material properties of GOTHIC thermal conductors.

Specification	Database	GOTHIC LP	GOTHIC 3D
Total free volume (m³)	73944.46	73944.46	74108.05
Steel mass (kg)	4.4371E+06	4.4371E+06	4.4527E+06
Steel volume (m³)	563.84	563.84	574.33
Steel surface area (m²)	32106.77	32106.77	32101.54
Concrete mass (kg)	4.6624E+07	4.7263E+07	4.7283E+07
Concrete volume (m³)	18649.66	18905.26	18913.24
Concrete surface area (m²)	36303.90	36303.90	36305.73
Material properties (value at 100 °C)	Density (kg/m³)	Conductivity (W/m.K)	Specific heat (kJ/kg.K)
Carbon steel ANSI 1010	7752.90	44.23	0.47
Concrete	2500.00	1.76	0.90

4. Application Case: Total Loss of AC Power with Late Depressurization

Within AMHYCO's WP2, several project partners submitted full-plant SA simulations. The M&E release rates were then used in WP4 to feed the containment models based on the generic containment database (Herranz and Fontanet, 2023). The transient chosen for this paper comes from a simulation of a Station Black-Out (SBO) accident in a PWR-KWU, where the primary depressurization of the RCS is delayed, in comparison to the request of the emergency manual. The transient was simulated with MELCOR and the M&E sources from the RCS are treated as external sources in GOTHIC. This is done by means of several boundary conditions, located in the SG-N region for the LP model, and in specific cells of the equipment rooms CV in the 3D model (at the top elevation of the pressurizer relief tank, where the overpressure protection rupture disk is located). In more detail, the studied sequence is a loss of offsite power (LOOP), after which the plant cannot switch to house-load operation and subsequently all diesel generators fail to start. Thus, the plant suffers a total loss of all sources of AC power in an SBO situation. For the first hour after the initiating event, the decay heat is removed by the dry-out of the steam generators. Thereafter, the pressurizer safety valves start cycling, discharging large amounts of steam into the pressurizer relief tank. The relief tank cannot cope with the influx of coolant indefinitely, and subsequently the rupture disk breaks,

releasing steam into the containment. With the decreasing inventory in the primary loop, the core outlet temperature reaches 650° C after about 2 h 10 min, where the SAMG issue the call for RCS depressurization. It is assumed that after another 30 min the pressurizer safety valves are manually/remotely opened to reduce primary pressure. At this point in time (2 h 40 min), already a significant mass of H_2 is stored in the primary loop, which is released in a short period by the depressurization through the pressurizer relief tank into the containment. With decreasing primary pressure, the hydro-accumulators start injecting, temporarily flooding the reactor core. After the depletion of the hydro-accumulators, the core begins to dry out and eventually melts, the vessel then fails at about 9 hours. Fig. 6 shows the release rate boundary conditions for the containment response simulation, namely steam and H_2 mass flows into the containment, as well as the relief tank pressure and temperature at the injection.

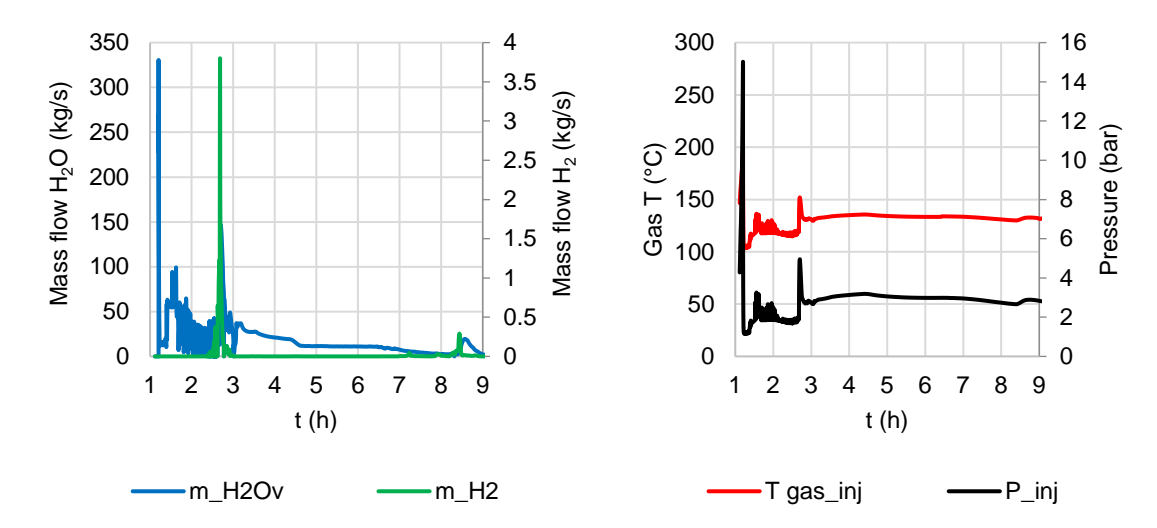


Fig.6. Released mass of steam and H₂ (left), release pressure and gas phase temperature (right).

In the following Section 4.1, the "unmitigated" (without considering PARs) accident progression is firstly studied by means of the LP model simulation. Then, a comparison regarding thermal hydraulic variables and combustion risk thresholds is performed between the LP and the three parametrically equivalent 3D models. The observed differences between the approaches were highlighted and the plausible sources of discrepancy were classified. Moreover, one of the 3D models is chosen to study the H₂ concentration and combustion risk at the region, room and sensor level. Finally, in Section 4.2, the "mitigated" scenario is compared for the LP and the 3D baseline model, by evaluating the total recombination rates yielded by the PAR layout, the behavior of the PAR components under each approach, and the reduction on the flammable clouds and in turn of the combustion risk. The simulations were performed on an 8 core CPU (i7-9700@3.0GHz) with a maximum time step of 0.04 seconds. Results are shown from hours 1 to 9 of the transient (start of M&E release and end of in-vessel phase, respectively).

4.1 Results for the unmitigated scenario

4.1.1 LP model results

For the studied unmitigated scenario, the accumulation and subsequent condensation of the released steam is the main driver for the pressure evolution, especially during the first hours of the transient (Fig. 7 left). Indeed, in the first half of the sequence, high condensation rate peaks were found at the DOME region, whose trends matched the heat transfer rates between UJA and UJB regions throughout the steel liner (Fig. 7 right). In detail, condensed steam was quickly replaced by the

upcoming releases and an ascending portion of the remaining non-condensed inventory from the equipment rooms. Moreover, a total of 178 MJ of thermal energy was evacuated from the UJA accessible rooms during the whole transient, largely contributing to the pressure stabilization. Furthermore, the second greatest condensation rate was achieved in the SUMP region, the principal driving mechanism being the surface condensation over the accumulated water pool.

Then, Figure 8-left shows the buildup of steam after the release cycles at 6 representative regions of the 10 defined at the UJA nodalization, where the SUMP, SG, and DOME regions reached concentrations up to 80%. Contrarily, the annular compartments and the DUCT region, which are the furthest from the break location, remained rather isolated from the main convection loops generated when the steam and NCGs crossed the steam generator towers and reached the DOME region. Also, the RROOM region (above the cavity and connected to the SG regions with small window-type junctions) accumulated lower concentrations of steam than the rest of the regions inside the shrapnel cylinder. Therefore, these latter regions presented lower temperatures, whereas the part of the steel liner which bounds the DUCT and ANN regions yielded lower heat transfer rates to the UJB building. Thus, these outer rooms accumulated higher H₂ concentrations over the sequence, and their atmosphere was denser because of the colder initial air inventory. Nevertheless, following the main steam release after the 3-hour mark, H2 volumetric concentration stabilized between 4-5 % for the equipment and accessible rooms (see Fig. 8-right). From that point on, steam condensation was the main contributor to the pressure stabilization observed on Figure 7-left, until the last steam inventory was released at 8.5 h, slightly re-pressurizing the containment (although maximum pressure, 3.81 bar, is reached at 4.5h). Finally, Figure 9 shows an assessment of the H₂, steam and NCGs accumulation within the aforementioned LP regions, using a Shapiro-Moffette ternary diagram (Shapiro and Moffette, 1957). The point representing the mixture's composition on the diagram is used to determine whether the gas cloud can suffer a slow deflagration or possible flame acceleration (Bentaib et al., 2010). Then, as a first approach, the diagram area where a combustion event is plausible is delimited with pre-established H₂ flammability limits (Herranz and Fontanet, 2023; Martín-Valdepeñas et al., 2007), which at the right of the figure. As can be seen, all regions except the DUCT entered the combustion risk domain at the diagram, the RROOM region being in flammable conditions for the most part of the sequence as it accumulated the higher H₂ relative concentrations.

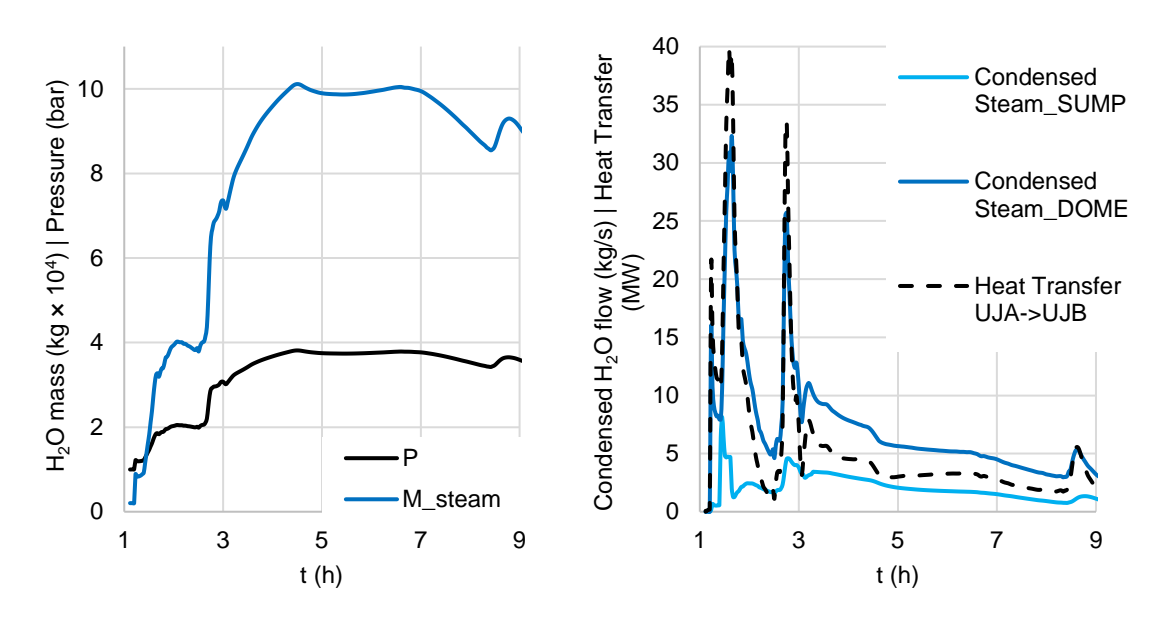


Fig.7. Pressure and accumulated steam mass within the containment (left), condensed steam rates at DOME and SUMP regions and heat power transferred between UJA and UJB buildings (right) for the SBO LP unmitigated simulation.

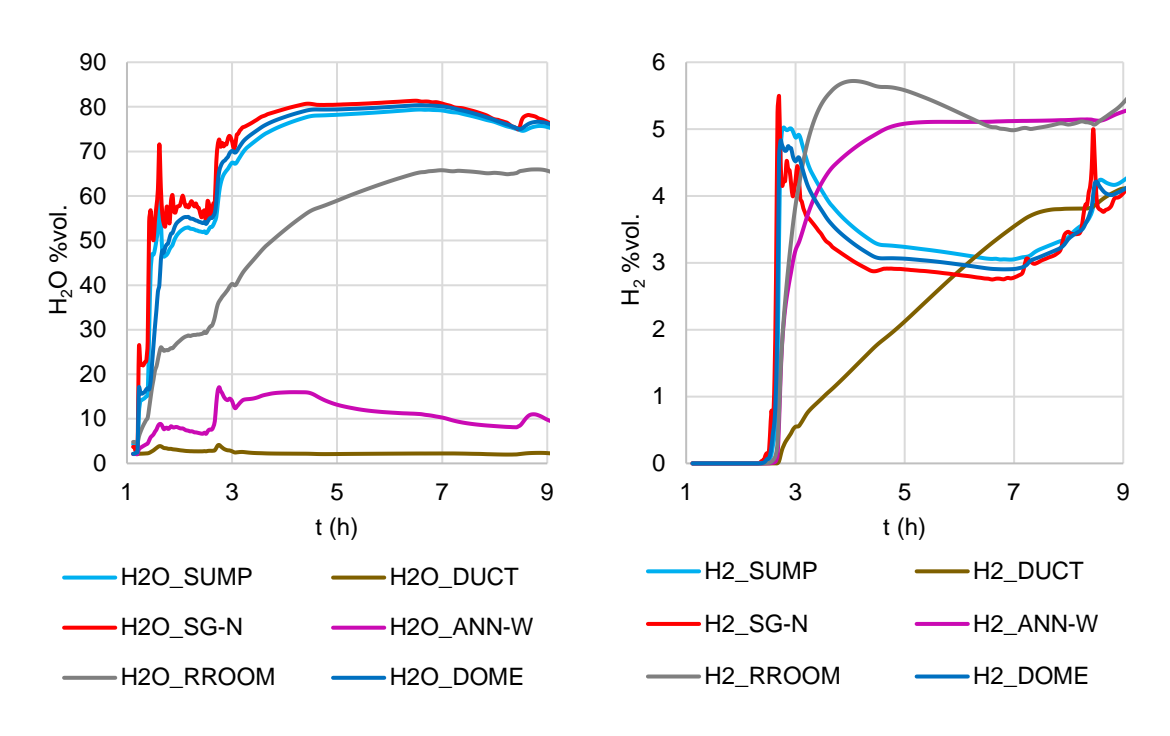


Fig.8. Volumetric concentration of steam (left) and hydrogen (right) for the SBO LP unmitigated simulation.

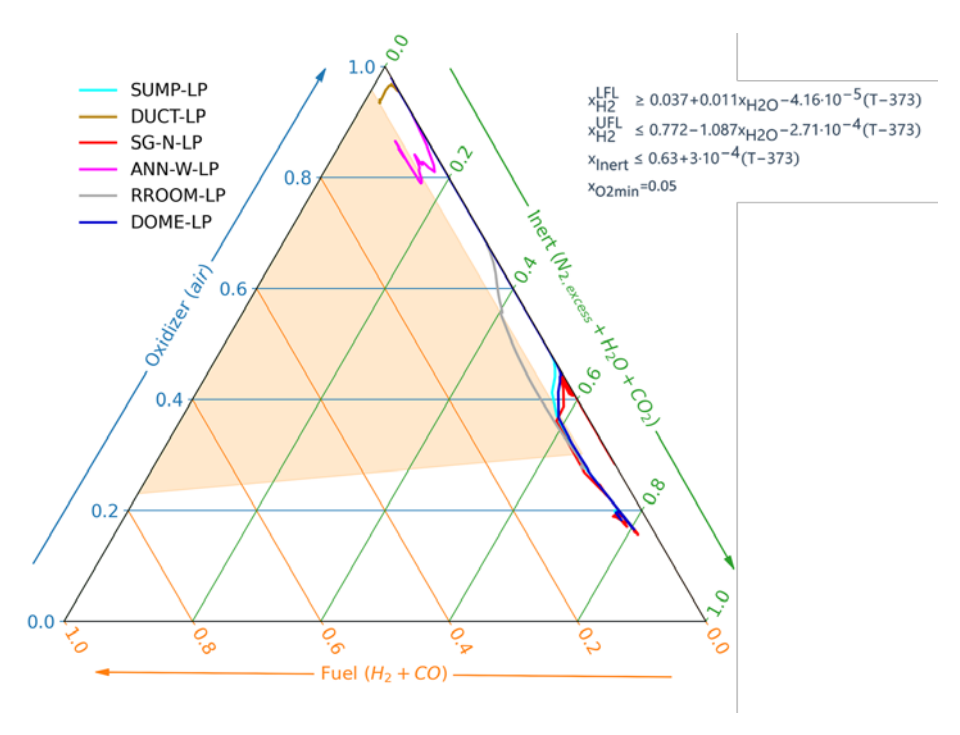


Fig.9. Containment conditions for hydrogen deflagration within six regions for the SBO LP unmitigated simulation.

4.1.2 Comparison of LP and 3D results - Global averaging 'regions'

In the following, several figures of merit of the main regions of the containment are compared for the unmitigated LP case and the respective 3D simulations with different meshing ('3D-30k', '3D-60k', and '3D-80k'). The objective is to detect relevant deviations between these approaches and correlate them to avoidable or unavoidable effects. The simulations lasted 0.87 hours for the LP model, and 5.6, 10.3, and 20.1 days for the '3D-30k', '3D-60k', and '3D-80k' models, respectively, using CPU 8 cores (i7-9700@3.0GHz). To compare GOTHIC LP to 3D outputs, which are given on a cell level, these must be averaged to the respective UJA region that replicates each LP CV. This is performed with an in-house ProTON code that identifies the coordinates of each cell and assigns them in their respective region (user-defined, as per the original coordinates of the generic containment database regions).

Figure 10-left shows the containment pressure evolution for the different approaches. In general, the results of the 3D and LP approaches were close. As the transient evolves, the 3D models predicted a higher containment pressure, and therefore containment steam total mass content (Fig. 10-right), especially after the primary depressurization at 2 h 40 min, with a maximum relative difference of 6.7% (30k), 8.5% (60k), and 10% (80k), respect to the LP calculation. The main driver for this difference is the total condensation rate, which decreased with increasing mesh refinement. Compared to LP calculation, the '3D-30k' model condensed ~1% less steam, while the '3D-60k' and '3D-80k' models generated ~3% less condensate. Nevertheless, condensation over the TC surfaces was slightly higher for the 3D simulations at some stages of the sequence, e.g., peaks at the steel liner after 2 h 40 min not seen by the LP calculation.

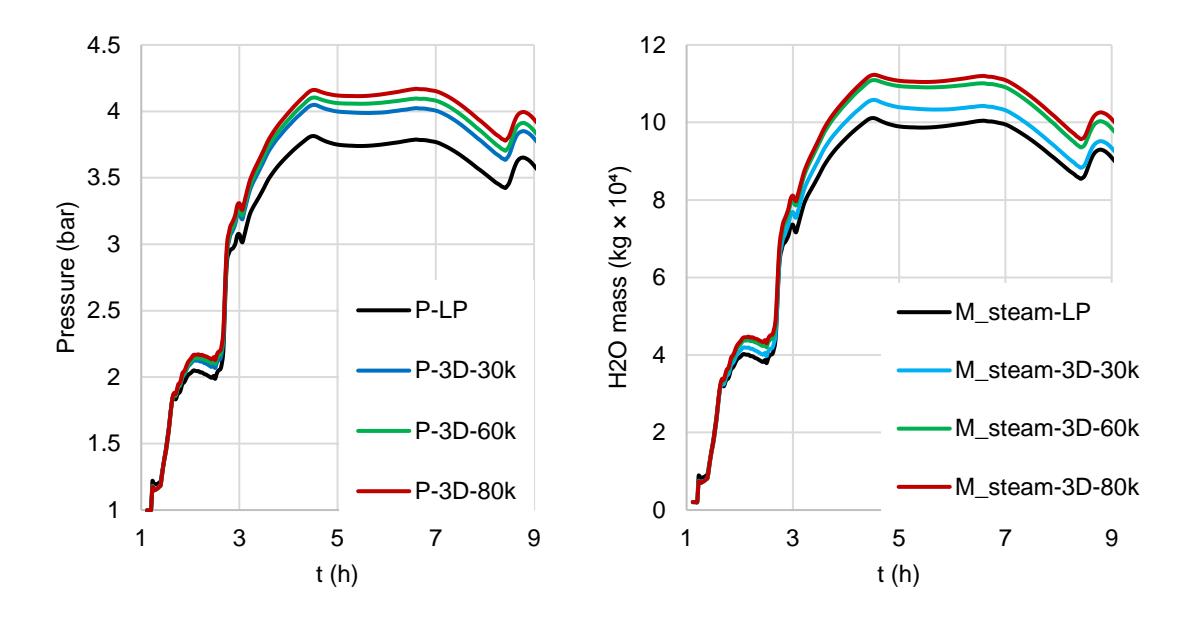


Fig. 10. Containment pressure evolution (left), and steam mass content (right) for the LP vs. 3D SBO unmitigated scenario.

Although heat transfer rates were close to the LP ones (see Fig.11-left), the 3D models transferred around 4% more thermal energy through the liner (accumulated MJ up to the end of the sequence) than the LP one. Then, although the steel shell may act as a slightly more powerful heat sink in the 3D models, the source of deviations affecting the pressure seemed to have its origin in the

condensation profiles at different regions of the containment. These deviations were maintained through the pressure stabilization periods. Furthermore, condensation over water pool surfaces, especially within the SUMP region, was the mechanism explaining the higher condensation and lower pressure for the LP model (see results for the SUMP and DOME regions at Fig. 11-right). Moreover, the steam reaching an LP region gets in contact with all the pool free surface at once for each time step, while for a 3D calculation the heat balance between the region atmosphere and the pool can give different local condensation profiles depending on local conductor temperatures.

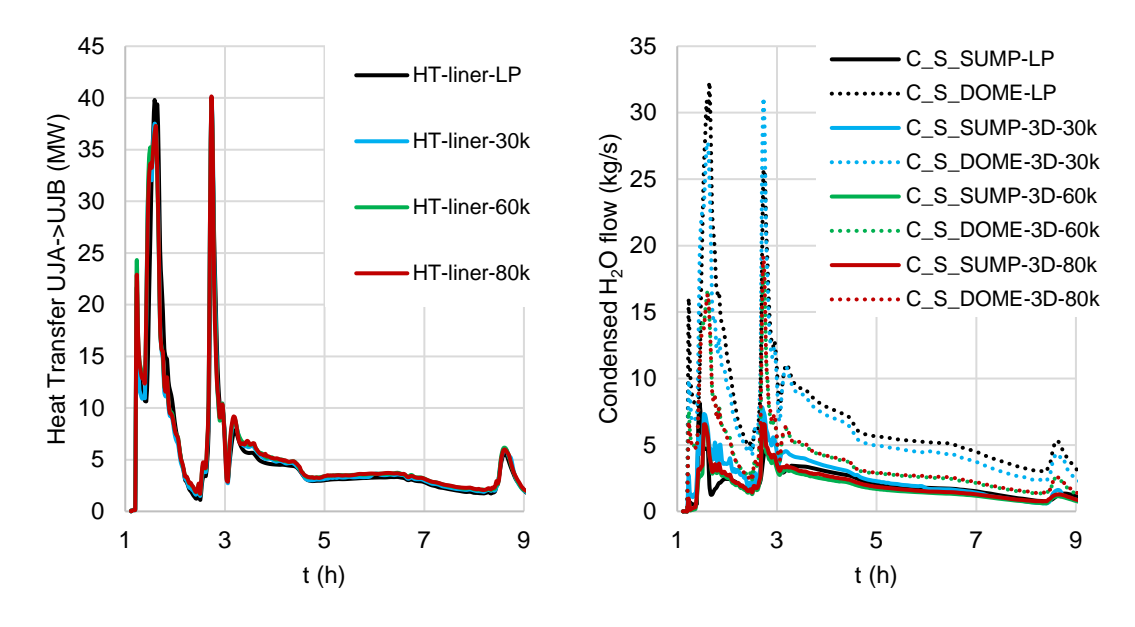


Fig. 11. Heat power transferred between UJA and UJB buildings (left), and condensed steam rates at DOME and SUMP regions (right) for the LP vs. 3D SBO unmitigated scenario.

In Fig. 12, the distribution of the gas mixtures in the containment is assessed in more detail (3D results averaged on the scale of regions), as predicted both by LP and 3D codes. Thereby, Fig. 12-left shows the SUMP region, and Fig. 12-right the DOME one. For the latter, steam and H₂ concentration trends were coherent, with small deviations between the LP and '3D-30k' approaches and the other two 3D models. Contrarily, the SUMP region showed higher variations in the gas mixture concentrations (e.g., H₂ peaks at the '3D-30k' model just after the first H₂ release coming from the above SG-N region), which could be due to the small deviations in the condensation profiles, both over TC surfaces and over the pool of water formed in the containment sump. It is important to notice that the representation of some volumes, such as the SUMP and the DOME, as large LP regions may underestimate high local concentrations of gases and locally high temperatures. This is an intrinsic issue of the LP approach, which foresees an instantaneous dilution of any gases within a control volume; the larger the region, the more likely does a significant underestimation occur (OECD, 2007). Moreover, it seems that coarsening the mesh of the regions inside the cylinder (such as the SUMP) for the '3D-30k' model, significantly influenced the flow distribution there, compared to the finer meshes.

Finer nodalizations would enable to better capturing the momentum balances and form losses throughout the paths followed by the gas mixture over the different convection loops, as well as local heat transference peaks between colder surfaces and hotter gas streams. This could be especially beneficial for the ANN-E and ANN-W regions, which are separated between inner- and outer-cylinder rooms in the 3D models. However, discrepancies are expected to arise due to the differences in the nodalizations and the inherent assumptions within each approach, which would translate in deviations

in the transport of the fluid phases between the numerical cells in the 3D model or CVs in the LP model.

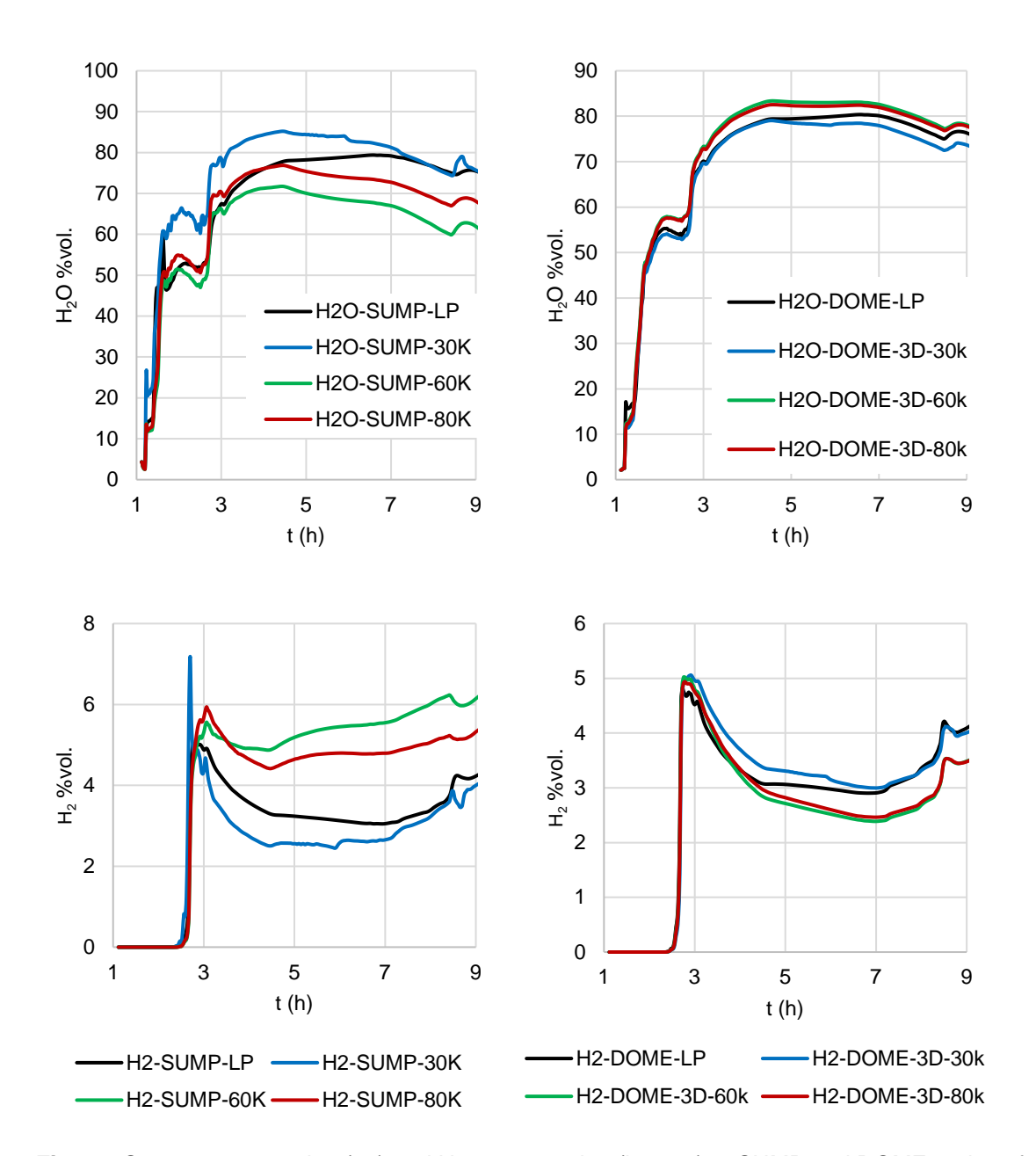


Fig. 12. Steam concentration (up) and H₂ concentration (bottom) at SUMP and DOME regions for the LP vs. 3D SBO unmitigated scenario.

LP and 3D models also delivered generally consistent results in the Shapiro-Moffette diagram (Fig. 13). The deviations might be directly traced back to the variability of the prediction of the H₂ and steam concentrations within the respective regions. For instance, big regions like the DOME showed a closer agreement than the SUMP one, where H₂ concentrations showed higher variability. Also, the SG-N region entered in the flammable domain earlier than the 3D models, whereas for the RROOM

region, that was the case for the '3D-30k' model (Fig. 13-bottom). These different behaviors in each region led to a more precise evaluation of the actual flammable clouds formed in the containment, in terms of mass and volume of the gas phase at flammable conditions. However, that calculation may be highly influenced by the chosen post-processing scheme, as averaged values over big regions might hide local harsher conditions which would add up to the possible global flammable volume.

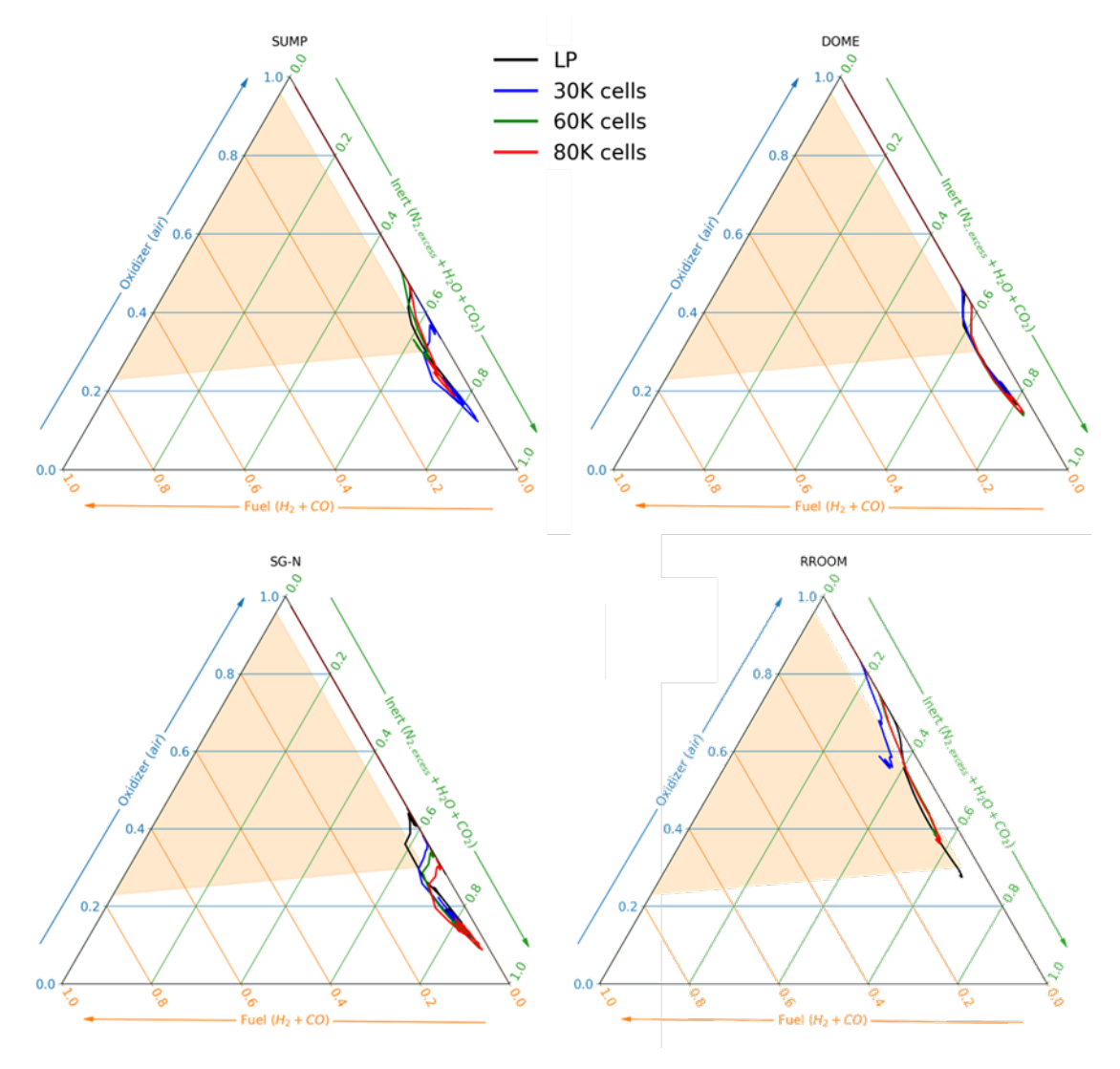


Fig. 13. Containment conditions for hydrogen deflagration at SUMP (up-left), DOME (up-right), SG-N (bottom-left), and RROOM (bottom-right) regions for the LP vs. 3D SBO unmitigated scenario.

4.1.3 Comparison of LP and 3D results – Total flammable volume at the region, room and cell scales

To quantitatively assess flammability during the simulated sequence, the ProTON code was used to evaluate whether gas mixtures within the LP and 3D calculations exceeded flammability limits. The code identifies gas cloud volumes and masses within the containment that could sustain combustion following an assumed ignition, based on local gas concentrations. It distinguishes between slow and fast deflagration potential, the latter assessed via the sigma criterion for flame acceleration in already flammable cells (Dorofeev et al., 2001; OECD/NEA, 2000; Vázquez-Rodríguez et al., 2025). For an

LP calculation, each CV is flagged as flammable (assigned a value of 1) only if the entire volume meets the required conditions, a limitation of coarse spatial resolution. For 3D models, the same evaluation is applied at the cell level or to sets of cells corresponding to the free volume of LP CVs. Alternatively, flammability can be assessed across the smaller 3D rooms comprising each region (Fig. 2), enabling a more spatially resolved analysis.

The evaluation was initially conducted at the region level to estimate the total flammable volume within the containment over time (Fig. 14-left). At 2.7 h, following the first H₂ release, rapid gas distribution to upper regions led to over half of the containment being temporarily classified under slow deflagration conditions—captured consistently by both the LP model and 3D meshes using region-averaged values. Initially, the LP scenario yielded a higher total flammable volume, but 3D models showed close agreement and exceeded the LP prediction around 6 h into the accident. Notably, the '3D-60k' model displayed the highest cumulative flammable volume at the end of the simulation, indicating more widespread severe conditions. Subsequently, region-averaged data in the 3D models were refined using room averages of constituent cells, and the analysis was repeated at cell level. While room-averaged results remained consistent with region-level and LP estimates, cell-level evaluation revealed transient flammable pockets earlier in the sequence and slightly increased volumes for finer meshes at later stages (Fig. 14-right). In contrast, the '3D-30k' model produced lower flammable volumes, suggesting that room and region averages may have overpredicted flammability in some areas. This outcome is also attributed to lower H₂ concentrations in the SUMP region, which contributed more significantly to the other two 3D meshes.

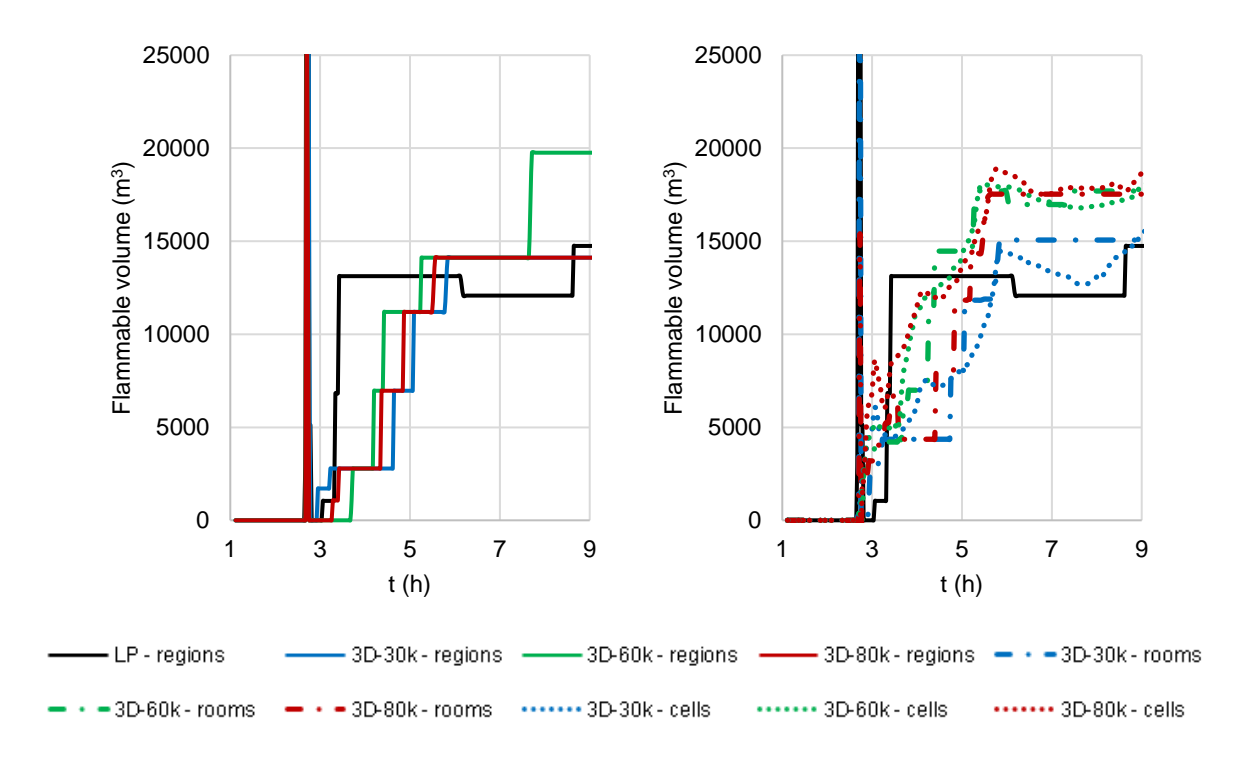


Fig. 14. Volume of containment in conditions for possible slow deflagration for the LP vs. 3D SBO unmitigated scenario using averaged region output (left), local averages and 3D cell data (right). Total containment free volume is ~74.000 m³.

To elucidate the contribution of individual regions to the total flammable gas volume, a finer spatial analysis was conducted for the 3D models using ParaView (Ahrens et al., 2005), as shown in Fig. 15.

Cross-sectional views of gas concentrations across the 3D meshes revealed localized H_2 accumulations at scales smaller than those captured by the LP or region-averaged 3D volumes. To investigate these patterns in greater detail, one 3D model was selected for an in-depth assessment of flow behavior and gas distribution. Based on previous results, global metrics showed good agreement between the coarser models (LP and '3D-30k') and between the more refined ones ('3D-60k' and '3D-80k'). Among them, the '3D-60k' mesh produced intermediate results and offered a favorable balance between resolution and computational cost—requiring only half the runtime of the finest mesh. Consequently, this model was selected for further detailed analysis of containment behavior at finer scales.

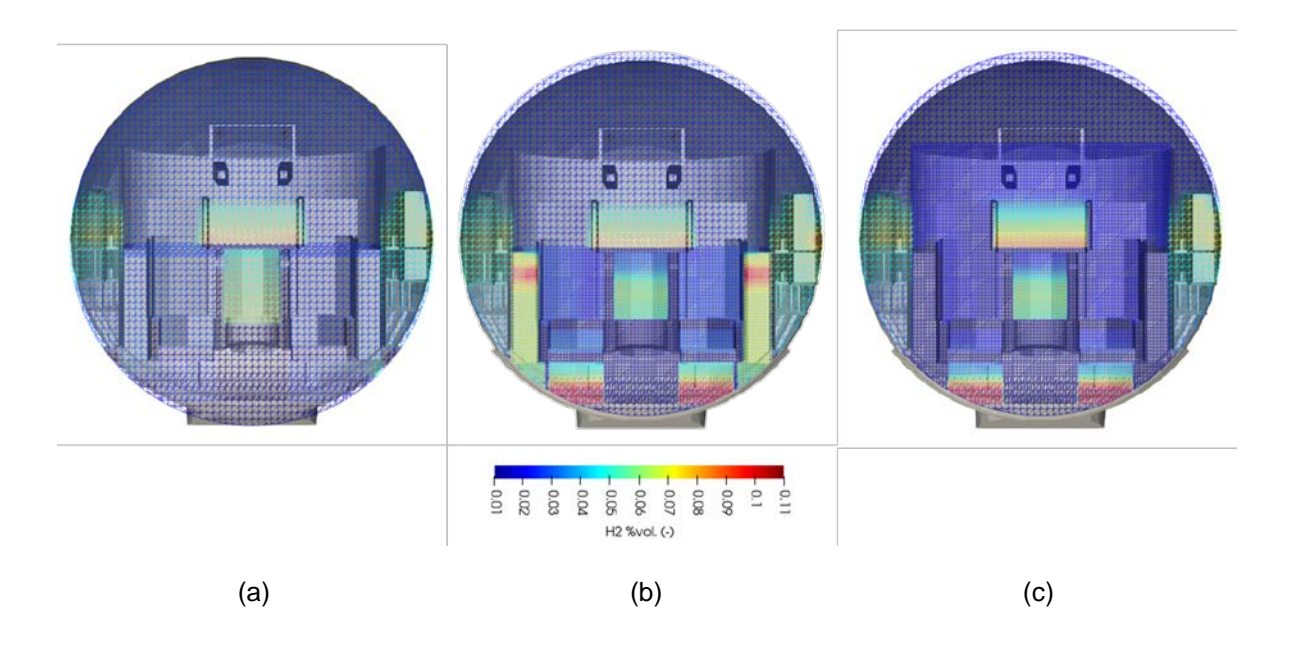


Fig. 15. H₂ distribution (at 4.5 h) in containment for the '3D-30k' (a), '3D-60k'(b), and '3D-80k' (c) for the 3D SBO unmitigated scenario.

4.1.4 3D H₂ concentration and combustion risk - Local averaging and cell values

The volumetric concentration of H_2 was re-evaluated at the room and cell levels and compared to the region averages of the '3D-60k' simulation. The objective is to look for local conditions within a few cells or a room that may not be visible when averaging over its mother region. Thus, H_2 concentration within the rooms which comprise the SUMP, SG-N, and DOME regions is depicted at Fig. 16, together with the corresponding Shapiro diagrams.

Thus, the SUMP region was split into three smaller rooms: the lower "Sump Basin" room (up to +6-meter elevation), and two upper compartments, "SUMP loop 1&2" and "SUMP loop 3&4" (see labels 11-13 in Fig. 2). When compared to the average region, the rooms showed a deviation of ±2 vol.% (Fig. 16-a), and a gradient developed with a hydrogen-rich layer at the bottom of the region. Indeed, the formation of such gradients is hidden in the LP approach and the 3D results averaged at the region level. For the rooms within the SG-N region, a more consistent behavior was drawn, (Fig. 16-c), except for the "Supply air duct" of the air recirculation system, which is a dead-end that do not participate in the in-containment convection loop. Again, a hydrogen-rich cloud entered the duct and got trapped there for a long time, doubling the volumetric concentration if compared to the region average, until the end of the transient. Concentration spikes (8 vol.% approx.) were observed at 2.5 h

(primary depressurization) and at ~8.5 h (core slumping), being the highest values at the "Pressurizer" room (see label 12 in Fig. 2), while when averaging over the entire SG-N region, the peak concentration dropped to ~6 vol.%. Regarding the rooms at the DOME region, there was a good agreement when comparing with the large fractions of the volume inside and outside the cylinder (Fig. 16-e). Here, the exception was the component rooms located on the operational floor (housing the pressurizer pilot-operated relief valves and recuperative heat exchangers, see label 33-35 in Fig. 2), which remained rather isolated and accumulated a tiny fraction of H₂. In general, the larger the 'averaging' room, the lower the peak values may become.

The different averages of H₂ volumetric concentrations (along with the rest of the gas mixture) also translated into varying combustion risk thresholds for the rooms and regions (Fig. 16 b-d-f). For instance, the "Sump Basin" room entered the flammability domain earlier, while the volumes closer to the pipes and the heavy concrete floor supporting the RCS equipment only briefly presented conditions for deflagration. For the SG-N region, only the "Supply air duct" stayed in the flammable domain for almost the entire in-vessel phase. For the DOME region, there were almost no flammable conditions identified either at the room or region level for the 3D simulation.

Furthermore, when evaluating concentrations at the cell level, where the measurement sensors are located (Fig. 2), it could be observed that the cell-wise values followed the room averages with reasonable accuracy (Fig. 17). The strongest deviation arose for the sensor "S9", located at the top of the pressurizer and close to the M&E release location. There, H_2 peak volumetric concentrations of 15% and 30% at 2,5 and 8,5 hours, respectively, were recorded. These corresponded to the release phases where a plume of H_2 started to dissipate within the containment atmosphere. Such a burst release can be identified (e.g. by the main control room) by the fact that the local gas measurement shows a peak, which then rapidly dissipates again on the time scale of ~20 min. Regarding the DOME sensor locations (S11-S13), measurements showed a concentration >6 vol.% during the initial release peak (due to the primary depressurization), while the room-averaged value remained at ~5 vol%.

Thus, even when the region and room-averaged values indicated no flammability (Fig. 16-f), there could be localized clouds of H_2 within the region at the burst release phase. As the dome is a large open area, an equilibration of the gas concentration can be expected with time, which is also reflected in the simulation. In the long term, the local measurements give a reasonably accurate picture of the H_2 concentration in the entire dome with a deviation of <1 vol%. Also, a possible misinterpretation based on the current H_2 detection points was observed. The monitor cell at the "pilot-operated relief valves" room (S10), located in a ceiling corner to detect a leakage from a pipe break on top of the pressurizer, only recorded a very small fraction of H_2 during the whole accident. Nevertheless, it emphasizes the fact that the main control room can be misled during an accident when focusing on the reading of an unsuitable H_2 sensor.

Then, to further understand the development of the compartment's thermal hydraulic conditions at all coordinates of the containment, post-processing of cell data was performed. As GOTHIC permits to export batches of output values readable by Paraview, several variables can be visualized in parallel. This allows for the identification of locally harsher conditions or hot spots that may be hidden in the coarser postprocessing averaging approach used up to now.

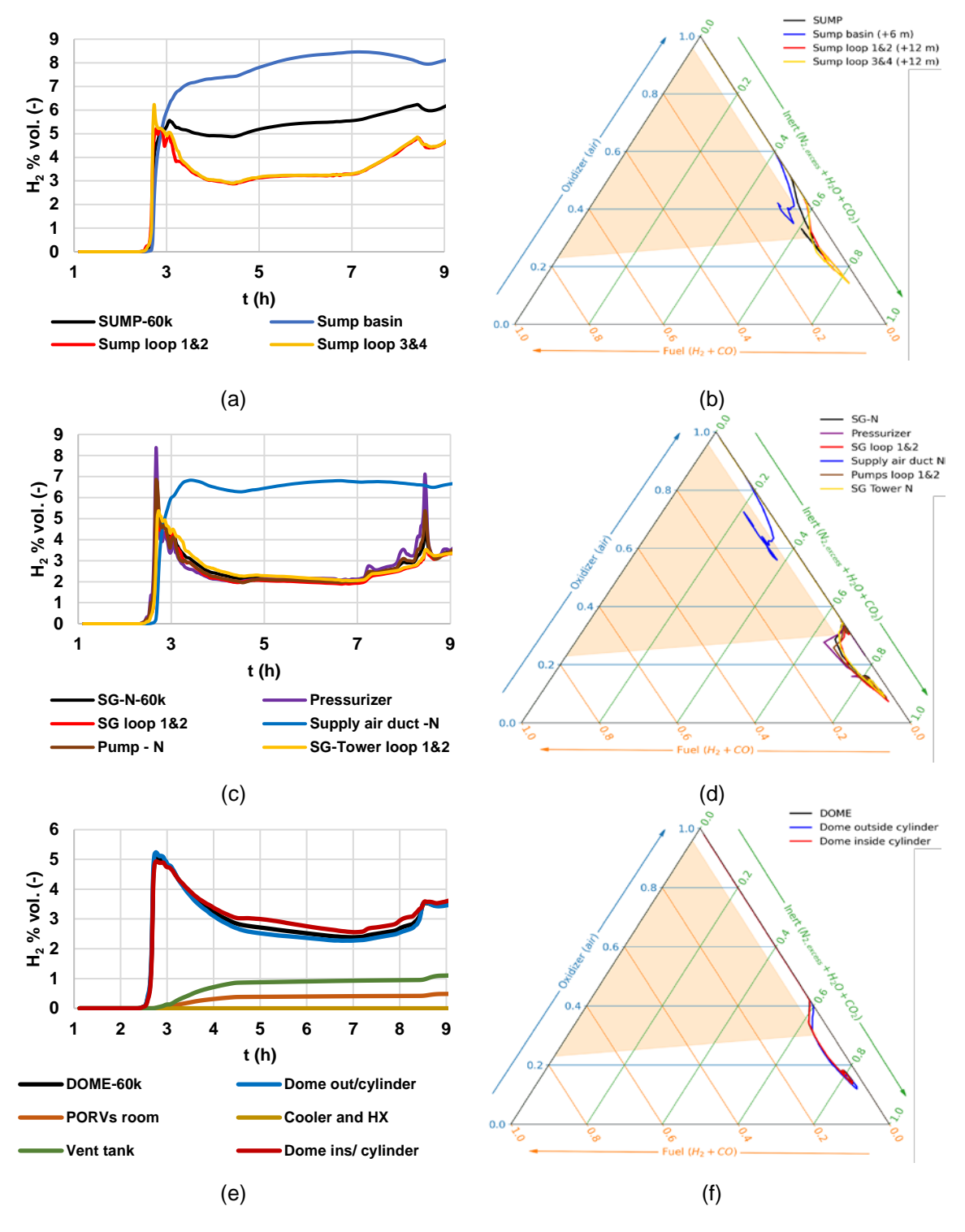


Fig. 16. Comparison of H₂ concentration on "regions" and "rooms" level for SUMP (a), SG-N (c), and DOME (e) volumes; qualitative conditions for combustion at SUMP (b), SG-N (d), and DOME (f) regions and selected rooms.

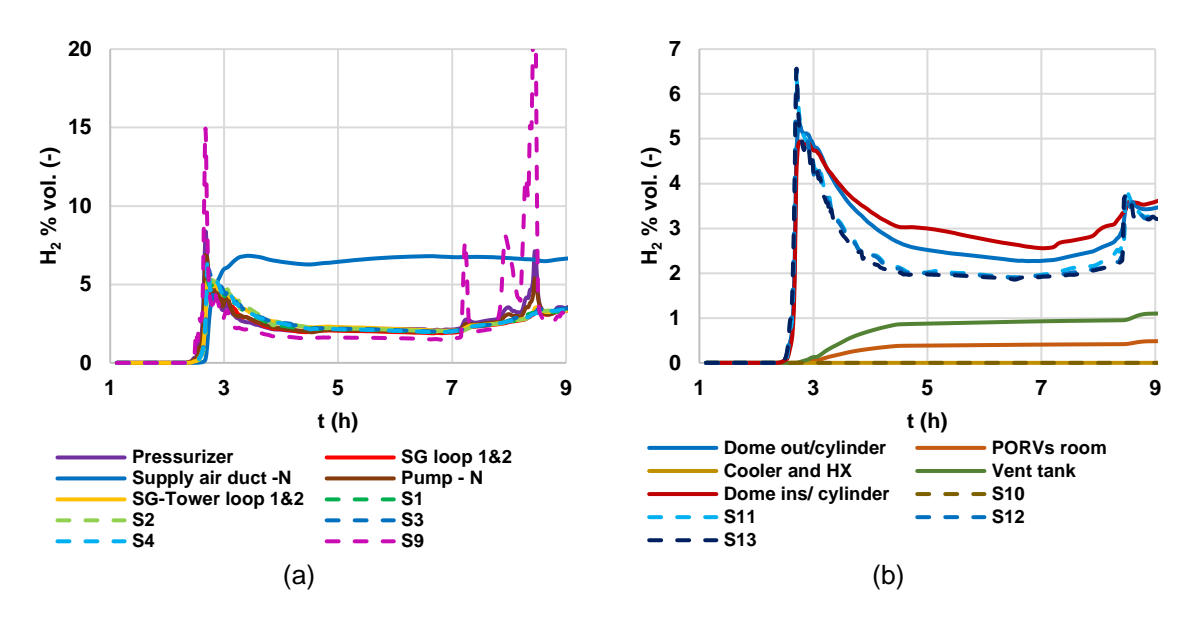


Fig. 17. Comparison of H₂ concentration between 3D rooms and selected cell data (measurement sensor locations) for SG-N (a), and DOME (b) volumes.

Thus, Fig. 18 gathers four sets of isovolume visualizations of H₂ volumetric concentration, steam volumetric concentration, and vapor phase density (steam and NCGs). Conditions were evaluated at 2.5, 4.5, 6.5 and 8.5 hours. Initially, at 2.5 h, a plume of hot gases rose from the SG compartments to the dome, where both H2 and steam began to accumulate. On the contrary, the outer annular compartments and the DUCT region did not participate in the in-containment convection loop, and thus remained colder and dryer, having a higher vapor phase density due to the higher air content (Fig. 18-a). With time, large amounts of steam were released and filled the DOME region cells, as well as the upper elevations of compartments within the equipment rooms, such as the reactor room or the sump (Fig. 18-b to d). This increased the density gradient between the compartments with initial higher concentration of air and the ones filled with steam. Also, as seen in the quantitative assessment, H₂ volumetric fraction was higher in the sump basin volume and in the supply air ducts (Fig. 18-b). However, the concentration at the ducts was higher at around the +18-meter elevation, while previously unidentified H₂-rich clouds were seen at the reactor room floor, at the HVAC air loop circulation rooms outside the cylinder, and at the operational floor first levels. Moreover, at 6.5 hours conditions homogenized at the supply air ducts and SUMP rooms, as well as for the annular compartments outside the cylinder and below the operational floor elevation.

The reactor room floor increased its H₂ concentration up to the end of the in-vessel phase. Then, at 8.5 hours, conditions homogenized even more, especially within the dome rooms, where large amounts of steam had been condensed on the colder surfaces (Fig. 18-d). A similar phenomenon was observed in the past at experiment validations (Wolf et al., 1999), and at comparable PWR-KWU models, something investigated thereafter as a possible instantiation of a sedimentation of H₂ provoked by a condensation profile under specific temperature and pressure conditions (Royl et al., 2009, 2000). To demonstrate that this phenomenon was indeed taking place, advanced characterization of each cell density and thermal hydraulic conditions, especially those adjacent to TC structures, would be needed to conclude if negative buoyancy flows are driving the lighter gases to lower levels (Liu et al., 2022). The occurrence of those local H₂ higher volumetric concentrations may also be related to higher condensation rates in the proximity of thick floors, such as on the reactor room floor connecting with the cavity, or at the operational floor slab.

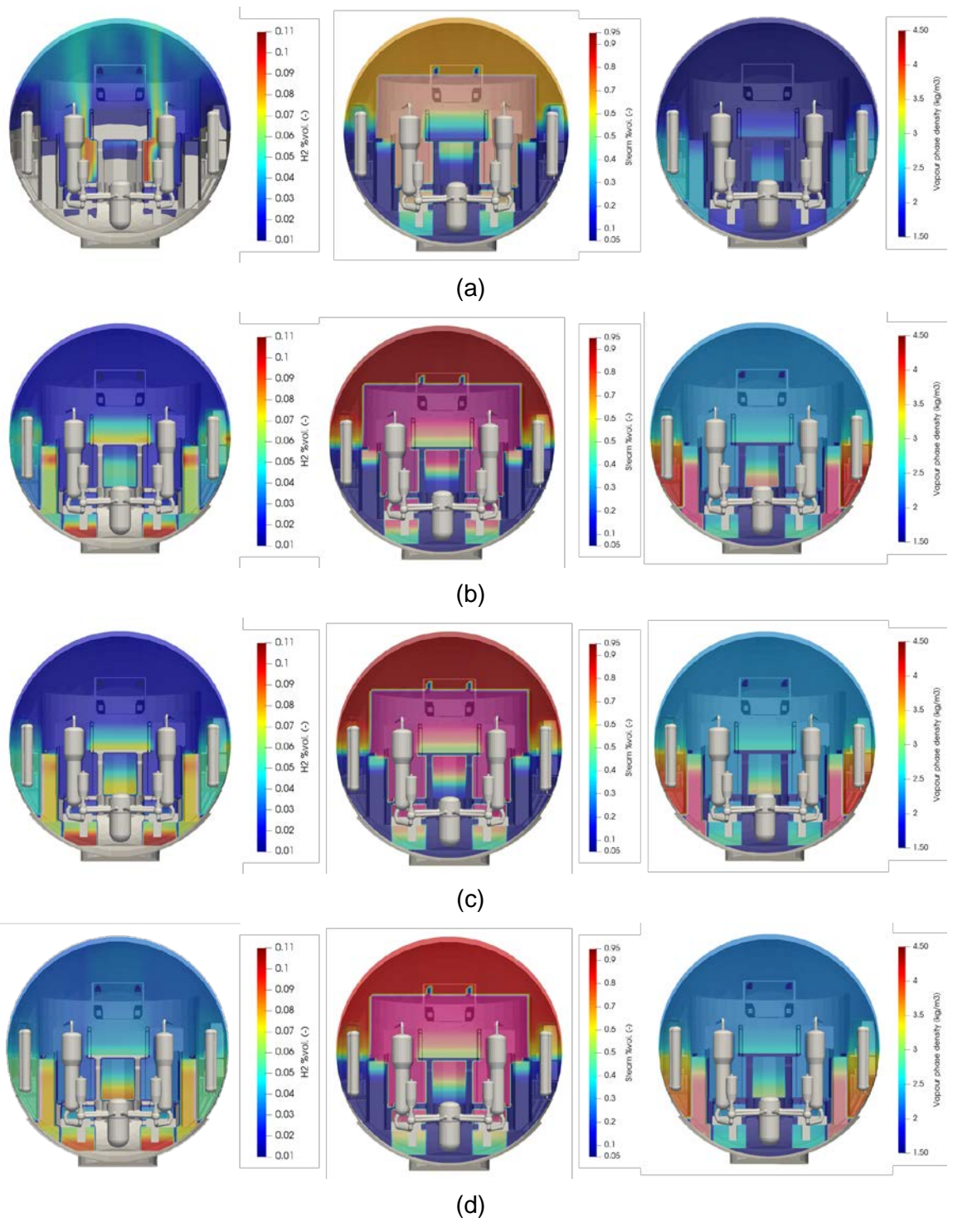


Fig. 18. Hydrogen, steam and vapor phase density contour slices inside the containment at 2.5 h (a), 4.5 h (b), 6.5 h (c), and 8.5 h (d).

Finally, a detailed visualization was performed at 4,5 hours of the in-vessel phase, where local high H_2 concentrations were identified in rooms such as the small equipment compartments at the inner annular compartments (Fig. 19). In general, the differences in the steam concentration on some volumes induced local accumulations of NCGs, temperature gradients, and heterogeneous condensation rates that configured some containment rooms as hotter and with higher relative humidities.

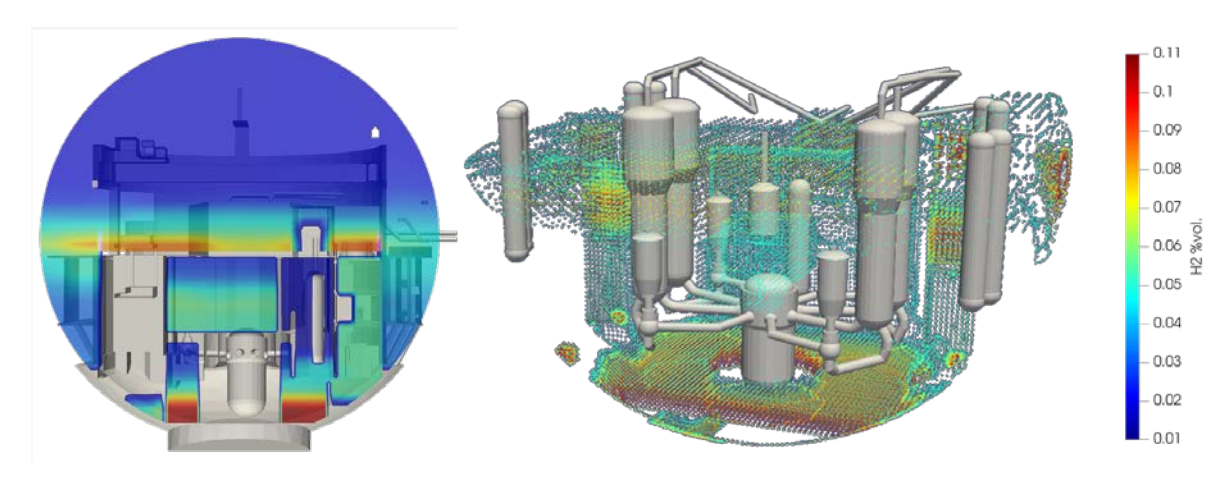


Fig. 19. Hydrogen distribution in the containment and local high concentrations at 4,5 hours.

4.2 Results for the mitigated scenario

The SBO sequence was simulated with an operative recombiner layout both in the LP and '3D-60k' models. As expected, during the simulation the PARs consumed a significant amount of the total released H₂ mass to the containment (705,5 kg). In detail, the LP simulation achieved a total recombination of 503.20 kg, being the recombined masses higher in the SUMP, SG-N, SG-S, ANN-W, and DOME regions, and obtained quicker, with respect to the 3D simulation. In contrast, the 3D regions recombined a total of 462.57 kg of H₂, 6.4 % less than the LP simulation but generally following similar trends (Fig. 20). The lower recombination rates of the 3D model could be due to not only temporarily lower concentrations of H₂ and O₂ in some rooms but also to the fact that the LP model exposes all PARs within a region simultaneously with a homogeneous H₂ concentration. Contrarily, the layout of PARs in the 3D simulation is subjected to the local gas-mixture flow streams traversing the cells of the PAR inlets, which may or may not be close to the main convection flows.

Table 4 details the total recombined H₂ mass between the LP and '3D-60k' approaches and compares it with the installed recombination capacity per region. For instance, regions such as the DUCT, which had a higher H₂ concentration at the 3D models, got their H₂ inventory more depleted in the mitigated sequences, whereas other regions which showed good comparability for the NCGs concentrations, such as the DOME, yielded much similar values. However, PARs in a region with less H₂ concentrations in the LP model can obtain higher recombination rates due to higher recombination efficiencies, such being the case of the SUMP. Another example is the RROOM region, where the 3D model, better captured the H₂ gradients between the inlet and outlet elevations of the PAR. In total, the recombined mass is quite comparable, i.e., the PAR capacity is large enough to compensate for the different local recombination rates (see Fig. 20).

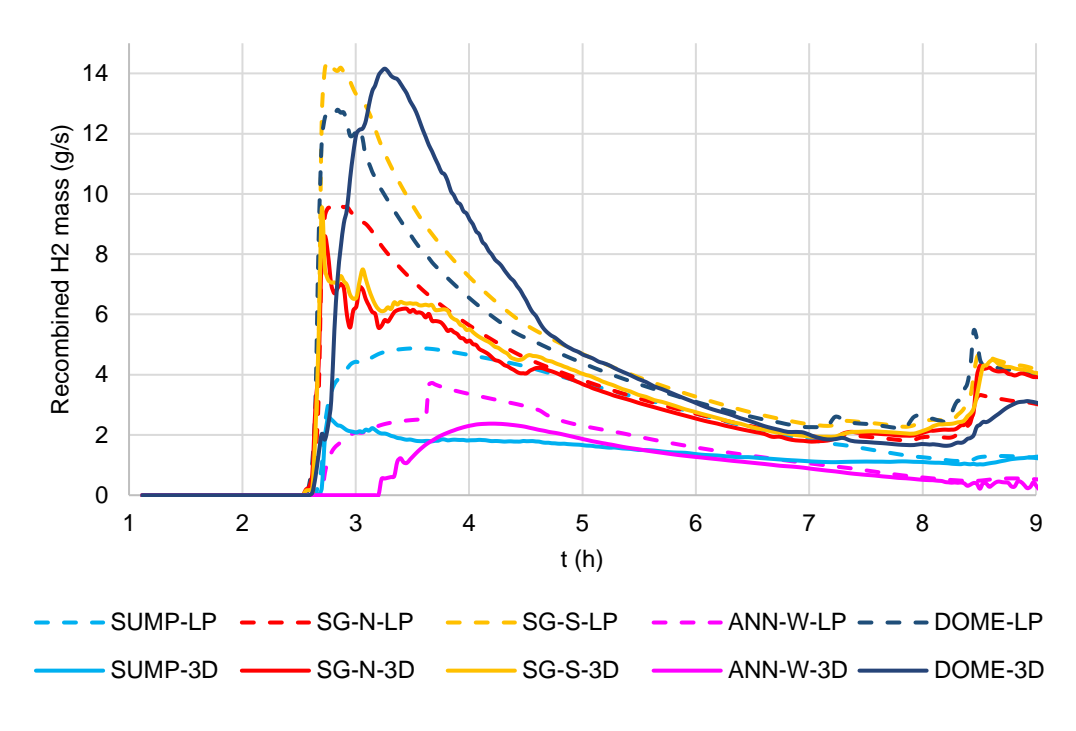


Fig. 20. Hydrogen recombination rates per region in the LP and 3D-60k simulations.

Table 4. Installed recombination capacity (at norm conditions) and total recombined mass, between GOTHIC LP vs '3D-60k' model approaches, up to the end of the SBO sequence.

Region	PAR installed capacity (kg/h)	Recombined H ₂ LP (kg)	Recombined H ₂ 3D-60k (kg)
SUMP	4.8	67.31	34.06
DUCT	21.44	25.53	60.55
SG-N	14.32	92.39	84.35
SG-S	14.32	121.24	89.80
ANN-E	13.12	38.42	46.97
ANN-W	13.12	38.42	25.71
RROOM	1.2	6.20	7.50
DOME	48.88	113.69	113.63
Total	131.2	503.20	462.57

Also, towards the end of the '3D-60k' mitigated simulation, the flammable gas volume decreased by 84% in comparison to the unmitigated scenario (Fig. 21-left). The remaining contributors to the flammable cloud in the mitigated case were the 'Sump Basin' and 'Supply-Air Duct' rooms. This resulted from the fact that in the dead-ends, where combustible clouds did accumulate, there were no PARs envisaged at the generic database. Finally, the operation of PARs, which work by an exothermic reaction, locally heated up the containment atmosphere. Temperature peaks were identified around the middle of the sequence and around the PAR outlets, e.g., at the SG regions (Fig. 21-rigth). There, hot plumes of steam and non-recombined H₂ and O₂ ascended to the upper levels, yielding local values of 170°C but rapidly cooling down to the surrounding temperature.

However, those values might exceed the environmental qualification criteria of the containment (European Commission, 1996; Jimenez et al., 2017), something that could be explored in detail by identifying the temperature maxima along the entire sequence and on similar scenarios.

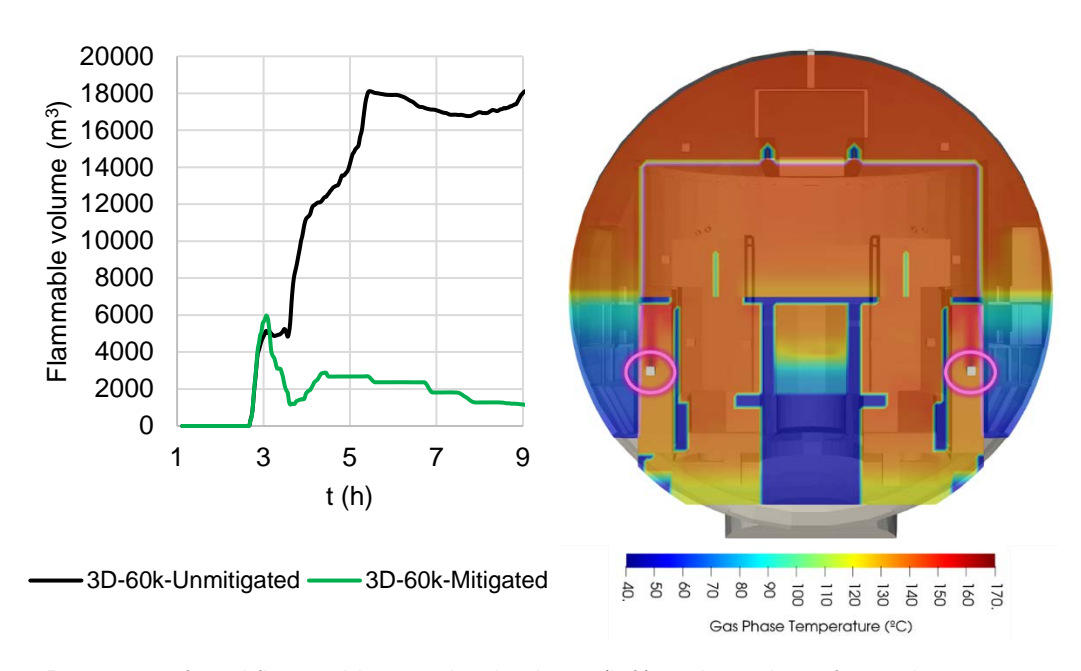


Fig. 21. Decrease of total flammable gas cloud volume (left) and cut view of gas phase temperature at 4 h. (right) at the mitigated 3D-60k scenario.

5. CONCLUSIONS

During the AMHYCO project, comparable LP and 3D models of a generic PWR-KWU containment were developed using the GOTHIC 8.3(QA) code. Both models were built from a shared geometrical database, with only minor code-specific adjustments. A comparative study was carried out under a SBO scenario—both unmitigated and mitigated with PARs—to evaluate the influence of modeling and post-processing strategies.

Such comparison, firstly revealed that the 3D meshes predicted slightly higher pressures, driven by lower total condensation rates. In detail, although condensation over the thermal conductor surfaces was generally higher for the 3D models, e.g., in the steel liner, where heat transferred from the UJA to UJB building was slightly higher, the LP model compensated with higher condensation over water pool surfaces, particularly at the containment sump region. Thus, LP models and coarse 3D meshes tended to yield visibly higher condensation rates in regions where liquid water was accumulated, which affected local flow patterns. This was seen for the coarse '3D-30k' model, where hydrogen distribution behaved differently than in the finer meshes, raising the question of the accuracy of coarser approaches to capture the flow patterns between certain regions.

Globally, it was deduced that the '3D-60k' model, consisting of approximately 60.000 computational cells, had intermediate results between the coarsest and finest meshes, as well as reasonable computation times with a level of geometrical accuracy close to the finer mesh tested, for what it was deemed optimal for further studies. As such, for the mitigated scenario, PARs were effective in reducing hydrogen inventory, significantly lowering the total flammable gas volume. LP and 3D models showed similar recombination trends per region, though the recombination rate was slightly

higher (~6 %) in the LP approach, in comparison to the 3D models, for this specific scenario. The 3D results are influenced by the interaction of local gas flows with the PAR inlets, depleting H₂ more effectively in higher-concentration regions, e.g., the pipeline duct. Also, temperature peaks, found particularly in SG regions and around PAR outlets, rapidly cooled down to surrounding temperatures

Furthermore, the simulations were evaluated under different post-processing scales (3D regions equivalent to LP volumes, 3D rooms, and individual 3D cells) to assess how post-processing schemes may affect the evaluation of combustion risk. A more detailed evaluation of the 3D results indicated that refining the post-processing method is valuable for two main reasons: (1) assessing whether the chosen averaging method influences key figures of merit, and (2) improving the representativeness of measurements that would be available in the Main Control Room. Indeed, some phenomena could be missed using only an LP code approach, such as hydrogen concentration peaks around the M&E releases that travel to upper regions. Also, the total gas cloud within flammable conditions in the containment showed a more complex behavior when analyzed using averaged values over small rooms and cell-wise data, compared to the LP values. Also, isolated sensors such as the one located in the PORVs room, revealed that local measurements can be far from the hydrogen concentration averages derived from a coarser spatial resolution. Similarly, hydrogen stratification at intermediate elevations was only captured when using room-level or finer averaging.

Overall, the comparison of LP and 3D calculations produced comparable results and trends, while some regions showed certain variability, contributing to distinct values of the mass of gas within flammable conditions. Then, the results demonstrated that systematic analysis of post-processing strategies, combined with mapping of spatial heterogeneities, can improve the accuracy of combustion risk assessments. The findings also show that 3D meshing can yield differences in predicted flammable cloud volumes and that cell-level or room-level post-processing enables the identification of zones that may remain relatively isolated during accident progression. An evaluation of the proportion of computational cells exceeding critical thresholds over time could support improved accident management and more effective placement of PARs and instrumentation. The post-processing methodology presented here provides a basis for future studies, including the evaluation of ex-vessel M&E releases across a range of sequences defined in the AMHYCO project.

DECLARATION OF COMPETING INTEREST

The authors declare that they have no known competing financial interests or personal relationships that could have appeared to influence the work reported in this paper.

DATA AVAILABILITY

The availability of the simulation input data used is subject to the regulations of the respective funding institutions responsible. The source code of the computational program used is confidential.

ACKNOWLEDGEMENTS

The AMHYCO project has received funding from the Euratom research and training programme 2019-2020 under Grant Agreement n°945057. The content of this paper reflects only the author's view. The European Commission is not responsible for any use that may be made of the information it contains.

GOTHICTM incorporates technology developed for the electric power industry under the sponsorship of EPRI, the Electric Power Research Institute. This work was completed using a GOTHIC license for educational purposes provided by Numerical Advisory Solutions, LLC. The authors also wish to

extend their appreciation to the personnel of EPRI and Numerical Advisory Solutions company for their invaluable technical assistance and support, especially to senior consultant Dr Jeffrey W. Lane.

REFERENCES

- Ahrens, J., Geveci, B., Law, C., 2005. ParaView: an End-User Tool for Large Data Visualization, Visualization Handbook (No. LA-UR-03-1560). Los Alamos Nuclear Laboratory.
- Allelein, H.-J., Arndt, S., Klein-Heßling, W., Schwarz, S., Spengler, C., Weber, G., 2008. COCOSYS: Status of development and validation of the German containment code system. Nuclear Engineering and Design 238. https://doi.org/10.1016/j.nucengdes.2007.08.006
- Bentaib, A., Caroli, C., Chaumont, B., Chevalier-Jabet, K., 2010. Evaluation of the Impact That PARs Have on the Hydrogen Risk in the Reactor Containment: Methodology and Application to PSA Level 2. Science and Technology of Nuclear Installations 2010. https://doi.org/10.1155/2010/320396
- Bocanegra, R., Jimenez, G., Fernández-Cosials, M.K., 2016. Development of a PWR-W GOTHIC 3D model for containment accident analysis. Annals of Nuclear Energy 87, 547–560. https://doi.org/10.1016/j.anucene.2015.10.022
- Braun, M., Reinecke, E.-A., Preprint Available at SSRN: https://ssrn.com/abstract=5199266.

 AMHYCO Engineering Correlation to Describe the Conversion of Flammable Gases in Framatome Passive Autocatalytic Recombiners. Nuclear Engineering and Design. https://dx.doi.org/10.2139/ssrn.5199266
- Dominion, 2006. Gothic Methodology for Analyzing the Response to Postulated Pipe Ruptures Inside Containment (Technical Report No. DOM-NAF-3-NP-A), Nuclear Analysis and Fuel Nuclear Engineering. Dominion Resources Services, Inc., Glen Allen, VA (USA).
- Dorofeev, S.B., Kuznetsov, M.S., Alekseev, V.I., Efimenko, A.A., Breitung, W., 2001. Evaluation of limits for effective flame acceleration in hydrogen mixtures. Journal of Loss Prevention in the Process Industries 14. https://doi.org/10.1016/S0950-4230(01)00050-X
- EPRI, 2018. GOTHIC Thermal Hydraulic Analysis Package, Version 8.3 (QA).
- EPRI, 2015. Fukushima Technical Evaluation, Phase 2— Revised GOTHIC Analysis. EPRI, Palo Alto, CA.
- European Commission, 1996. A comparison of European practices for the qualification of electrical and I&C equipment important to safety for European LWR nuclear power plant (No. EUR 16246), Nuclear Science and Technology. Standing Advisory Expert Group to the European Commission: Reactor Safety Working Group. European Commission, Luxembourg.
- Fernández-Cosials, K., Estévez-Albuja, S., Jiménez, G., Bocanegra, R., Vázquez-Rodríguez, C., Rey, L., Martínez-Murillo, J.C., 2019. 3D containment modeling of PWR-KWU Trillo NPP with the GOTHIC code. Annals of Nuclear Energy 133, 387–399. https://doi.org/10.1016/j.anucene.2019.05.041
- FRAMATOME, 2024a. WS85 In-Situ Containment Atmosphere Hydrogen Monitoring System Qualified for Loss-of-Coolant Accident and Fuel Pool Events. Framatome GmbH / PS-G-0634-ENG-201901. https://www.framatome.com/solutions-portfolio/docs/default-source/default-document-library/product-sheets/a0634-p-ge-g-en-0634-201901-ws85.pdf?sfvrsn=3625818b 2.
- FRAMATOME, 2024b. Passive Autocatalytic Recombiner Combustible Gas Control System. Framatome GmbH / PS-G-0642-ENG-202405. https://www.framatome.com/solutions-portfolio/docs/default-source/default-document-library/product-sheets/a0642-p-ge-g-en-202405-par.pdf?sfvrsn=ec8cb920_0.

- Harvill, R.C., Lane, J.W., George, T.L., 2021. Hybrid System Level and Coarse Grid CFD Tool for Three-Dimensional Natural Circulation, Mixing, and Stratification Modeling. Nuclear Technology 1–26. https://doi.org/10.1080/00295450.2020.1870371
- Herranz, L.E., Fontanet, J., 2023. D2.2 Identification and analysis of accident sequences with posing high H2/CO combustion risk (Deliverable Report, H2020 AMHYCO Project No. WP2-Task 2.2-2.4), Deliverable Report, H2020 AMHYCO Project. European Commission.
- Herranz, L.E., Jiménez, G., Kärkelä, T., 2025. Enhancing severe accident management through research. EPJ Nuclear Sci. Technol. 11. https://doi.org/10.1051/epjn/2025004
- Herranz, L.E., Jiménez, G., Nitti, F.S., 2022. Towards an optimized management of accidents. EPJ Nuclear Sci. Technol. 8. https://doi.org/10.1051/epjn/2022019
- Humphries, L.L., Beeny, B., Gelbard, F., 2017. MELCOR Computer Code Manuals (No. SAND2017-0876 O), Vol. 2: Reference Manual Version 2.2.9541 2017. Sandia National Laboratories, Albuquerque, NM 87185-0748.
- IAEA, 2011. Mitigation of hydrogen hazards in severe accidents in nuclear power plants. International Atomic Energy Agency, Vienna.
- Jimenez, G., Fernández-Cosials, M.K., Bocanegra, R., Queral, C., 2017. Analysis of the equipment and instrumentation qualification criteria using 3D containment models. Nuclear Engineering and Design 323, 28–38. https://doi.org/10.1016/j.nucengdes.2017.07.038
- Jimenez, G., Herranz, L.E., Bentaib, A., Chaumeix, N., Reinecke, E.-A., Kelm, S., Braun, M., 2022. AMHYCO PROJECT - TOWARDS AN ENHANCED ACCIDENT MANAGEMENT OF THE H2/CO COMBUSTION RISK, in: Proc. 19th International Topical Meeting on Nuclear Reactor Thermal Hydraulics (NURETH 19). Brussels, Belgium, 6 Mar 2022 - 11 Mar 2022.
- Kelm, S., 2019. SAMHYCO-NET. Proposal for the Generic Containment Code-to-Code Comparison (Task 'Generic Containment' No. Run-4.1 'State-of-the-Art PAR Model Application to the Ex-Vessel Phase'), SAMHYCO-NET. Forschungszentrum Jülich (FZJ), Jülich, Germany.
- Liu, F., Sun, Z., Cao, B., Bian, H., Ding, M., 2022. Numerical investigations on the component separation phenomenon and transport behavior of steam-air-hydrogen mixture induced by condensation. International Journal of Thermal Sciences 172, 107369. https://doi.org/10.1016/j.ijthermalsci.2021.107369
- Lopez-Alonso, E., Papini, D., Jimenez, G., 2017. Hydrogen distribution and Passive Autocatalytic Recombiner (PAR) mitigation in a PWR-KWU containment type. Annals of Nuclear Energy 109. https://doi.org/10.1016/j.anucene.2017.05.064
- Malakhov, A.A., Du Toit, M.H., Avdeenkov, A.V., Bessarabov, D.G., 2024. Numerical modelling of catalytic hydrogen combustion in passive autocatalytic recombiners: A review. Progress in Nuclear Energy 171, 105199. https://doi.org/10.1016/j.pnucene.2024.105199
- Martín-Valdepeñas, J.M., Jiménez, M.A., Martín-Fuertes, F., Fernández, J.A., 2007. Improvements in a CFD code for analysis of hydrogen behaviour within containments. Nuclear Engineering and Design 237. https://doi.org/10.1016/j.nucengdes.2006.09.002
- OECD, 2014. Containment Code Validation Matrix (No. NEA/CSNI/R(2014)3), Nuclear Safety. OECD-NEA.
- OECD, 2007. International Standard Problem ISP-47 on Containment Thermal-hydraulics, Final Report (No. NEA/CSNI/R(2007)10). OECD/NEA.
- OECD/NEA, 2014a. Status Report on Hydrogen Management and Related Computer Codes (No. NEA/CSNI/R(2014)8). OECD/NEA.
- OECD/NEA, 2014b. Assessment of CFD Codes for Nuclear Reactor Safety Problems Revision 2 (No. NEA/CSNI/R(2014)12). OECD/NEA.
- OECD/NEA, 2000. Flame Acceleration and Deflagration-to-Detonation Transition in Nuclear Safety (No. NEA/CSNI/R(2000)7), Nuclear Safety.

- Ofstun, R.P., Espinosa, R., Logan, C.P., 2013. Westinghouse Containment Analysis Methodology PWR LOCA Mass and Energy Release Calculation Methodology (No. WCAP-17721-NP). Westinghouse.
- Ofstun, R.P., Scobel, J.H., 2006. Westinghouse Containment Analysis Methodology (No. WCAP-16608-NP). Westinghouse, Pittsburgh, PA.
- Papini, D., Andreani, M., Ničeno, B., 2015. Simulation of Hydrogen Distribution in the Containment during a Severe Accident with Fast Hydrogen-Steam Release. Presented at the Proc. 16th International Topical Meeting on Nuclear Reactor Thermal Hydraulics (NURETH 16), Chicago, IL (USA).
- Papini, D., Andreani, M., Steiner, P., Ničeno, B., Klügel, J.-U., Prasser, H.-M., 2019. Evaluation of the PAR Mitigation System in Swiss PWR Containment Using the GOTHIC Code. Nuclear Technology 205. https://doi.org/10.1080/00295450.2018.1505356
- Royl, P., Rochholz, H., Breitung, W., Travis, J.R., Necker, G., 2000. Analysis of steam and hydrogen distributions with PAR mitigation in NPP containments. Nuclear Engineering and Design 202, 231–248. https://doi.org/10.1016/S0029-5493(00)00332-0
- Royl, P., Travis, J.R., Breitung, W., Kim, J., Kim, S.B., 2009. GASFLOW Validation with Panda Tests from the OECD SETH Benchmark Covering Steam/Air and Steam/Helium/Air Mixtures. Science and Technology of Nuclear Installations 2009. https://doi.org/10.1155/2009/759878
- Sehgal, B.R., 2012. Nuclear Safety in Light Water Reactors. Elsevier. https://doi.org/10.1016/B978-0-12-388446-6.00001-0
- Serra, L., Domínguez-Bugarín, A., Vazquez-Rodriguez, C., Jiménez, G., Kelm, S., Braun, M., Iskra, A., Cherednichenko, O., Herranz, L.E., 2023. D2.1 Data for the generic containment analysis (PWR-W, PWR-VVER, PWR-KWU) (Deliverable Report, H2020 AMHYCO Project No. WP2-Task 2.1), Deliverable Report, H2020 AMHYCO Project. European Commission.
- Shapiro, Z.M., Moffette, T.R., 1957. Hydrogen Flammability Data And Application To Pwr LossOf-Coolant Accident (No. WAPD-SC-545), Reactors Power. Westinghouse Electric Corporation, Bettis Plant. Pittsburgh, Pennsylvania.
- SIEMENS, 1990. Dokumentationen SIEMENS / KWU Sicherheitsbericht für die KKW Stendal GmbH 1990.
- Szabó, T., Kretzschmar, F., Schulenberg, T., 2014. Obtaining a more realistic hydrogen distribution in the containment by coupling MELCOR with GASFLOW. Nuclear Engineering and Design 269. https://doi.org/10.1016/j.nucengdes.2013.07.009
- Vazquez-Rodriguez, C., Bocanegra, R., Jimenez, G., Rey, L., Cadenas, A., Posada, J.M., Martínez-Murillo, J.C., 2019. Toward Conservatism in Containment Design Basis Accident Analyses. Lumped parameters and 3D Approaches. Presented at the ICAPP 2019 International Congress on Advances in Nuclear Power Plants, France.
- Vázquez-Rodríguez, C., Jiménez, G., Arfinengo-del-Carpio, S., Bocanegra, R., Domínguez-Bugarín, A., Serra, L., Estévez-Albuja, S., Fernández-Cosials, K., 2025. The Preventive Methodology: A priori modification of the containment geometry to boost the computational efficiency of GOTHIC 3D models. Nuclear Engineering and Design 432. https://doi.org/10.1016/j.nucengdes.2024.113718
- Visser, D.C., Siccama, N.B., Komen, E.M.J., Keij, T.L.J., 2015. HYDROGEN RISK ASSESSMENT -CFD MODEL VALIDATION AND REACTOR SCALE APPLICATION, in: Proc. 16th International Topical Meeting on Nuclear Reactor Thermal Hydraulics (NURETH 16). Chicago, IL (USA).
- Wolf, L., Holzbauer, H., Schall, M., 1999. Comparisons Between Multidimensional And Lumped-Parameter GOTHIC Containment Analyses With Data. Nuclear Technology 125, 155–165.

- Xiao, J., Travis, J.R., Royl, P., Necker, G., Svishchev, A., Jordan, T., 2016. Three-dimensional all-speed CFD code for safety analysis of nuclear reactor containment: Status of GASFLOW parallelization, model development, validation and application. Nuclear Engineering and Design 301, 290–310. https://doi.org/10.1016/j.nucengdes.2015.12.033
- Yu, F., Zhang, H., Li, Y., Xiao, J., Class, A., Jordan, T., 2018. Voxelization-based high-efficiency mesh generation method for parallel CFD code GASFLOW-MPI. Annals of Nuclear Energy 117, 277–289. https://doi.org/10.1016/j.anucene.2018.03.045